Supplementary Information for:

The chemistry of proton carriers in high-performance lithium mediated ammonia electrosynthesis

Hoang-Long Du, Karolina Matuszek, Rebecca Y. Hodgetts,
Khang Ngoc Dinh, Pavel V. Cherepanov, Jacinta M. Bakker
Douglas R. MacFarlane*, Alexandr N. Simonov*

School of Chemistry, Monash University, Clayton, Victoria 3800, Australia

*Corresponding authors:
douglas.macfarlane@monash.edu (DRM); alexandr.simonov@monash.edu (ANS)

TABLE OF CONTENTS

1. METHODS

Materials

Nickel wire (diameter 0.5 and 2 mm, ⩾ 99.9% trace metals basis) was purchased from Sigma-Aldrich. Lithium bis(trifluoromethanesulfonyl)imide ($LiNTf_2$; ⩾ 99%; HQ-115, LOT 10197) was purchased from 3MFluorad. Trihexyltetradecylphosphonium tris(pentafluoroethyl)trifluorophosphate ($[P_{6,6,6,1,4}][eFAP]$) was synthesised and purified following exactly the same procedures and using the same starting chemicals (1-ethyl-3-methylimidazolium tris(pentafluoroethyl)trifluorophosphate, $[C_2mim][eFAP]$, ⩾ 98%, from *Merck*; trihexyltetradecylphosphonium chloride, > 95%, CYPHOS or Sigma-Aldrich; dichloromethane, ⩾ 99.5%, *Merck*) as reported in our previous work.[1] Trihexyltetradecylphosphonium bis(trisflouromethylsulfonyl)imide ($[P_{6,6,6,1,4}][NTf_2]$) was synthesised following the same procedure as for $[P_{6,6,6,1,4}][eFAP]$, except that the $[C_2mim][eFAP]$ was replaced with $LiNTf_2$ and required 15 washes to remove the by-products and all NH_4^+, NO_3^- and NO_2^- contamination. Trifluoromethanesulfonimide ($HNTf_2$; ⩾ 95%) was purchased from Sigma-Aldrich. Methanol (analytical grade) was purchased from Merck. Ethanol (anhydrous, ⩾ 95%), n-propanol (⩾ 99.8%), isopropanol (anhydrous, 99.5%), n-pentanol (⩾ 99%) were purchased from Sigma-Aldrich. n-Butanol (analytical grade), tetrahydrofuran (stabilised with BHT, analytical grade), soluble starch and phosphoric acid (85 wt.%) were sourced from Chem-Supply. Other than drying procedure described below, these alcohols and THF were used as received. Deuterated tetrahydrofuran-d_8 (D, 99.5%), anhydrous ethanol-d_6 (D, 99%) and dimethyl sulfoxide-d_6 (DMSO-d_6; D, 99%) were obtained from Cambridge Isotope Laboratories Inc., UK. Ammonia solution, Sulfuric acid (98%) and acetone were supplied by Univar Solutions. NH_4Cl (> 99%), NaOH (pellets, analytical grade), salicylic acid (⩾ 99%), tri-sodium citrate dihydrate (analytical grade), sodium hypochlorite (10-15 wt.% chlorine), sodium nitroprusside dihydrate (⩾ 99%) and maleic acid (⩾ 99%) were purchased from Sigma-Aldrich and Merck. High-purity deionised water (Sartorius Arium Comfort I ultrapure water system H_2O-I-1-UV-T; measured resistivity 18.2 MΩ cm at 23 ± 2 °C) was employed in all steps that required water. High purity grade N_2 (99.999%; CO_2 < 1 ppm, O_2 < 2 ppm, H_2O < 2 ppm) and Ar (99.999%; CO_2 < 1 ppm, O_2 < 2ppm, H_2O < 2 ppm) gases were supplied by BOC Australia.

Electrochemical procedures

Electrochemical experiments were undertaken at ambient temperature (23 ± 2 °C) and 15 bar pressure in a gas-tight polyether ether ketone (PEEK) autoclave cell operated with a Bio-Logic electrochemical workstation in a three-electrode configuration.

Working electrodes bare nickel wire (Ø 0.5 mm; 0.15 cm^2) and isolated nickel wire (0.05 cm^2) were directly electropolished in a continuously stirred (Teflon-lined magnetic stirrer; 1000 rpm) phosphoric acid (85% aqueous solution) containing soluble starch (1:1000 w/v) for 2 min at an applied voltage of 5 V using a dc power supply (Powertech, MP-3091) before being used. In the electropolishing system design, a freshly cleaned 20 cm-long copper wire winded around the working electrodes into a helix was used a counter electrode. Afterwards, electropolished electrodes were immersed in absolute ethanol assisted by 5 min ultrasonication and dried with a compressed nitrogen blow gun.

Electrolyte solutions were prepared using tetrahydrofuran that was dried over activated zeolite "molecular sieves" (3 Å, Sigma-Aldrich) for 1 day and then stored over another fresh portion of activated zeolite in Ar-filled glovebox (Korea Kiyon; $O_2 \leq 0.6$ ppm and $H_2O \approx 0.0$ ppm levels were continuously monitored). Before use, the zeolite beads were washed with absolute ethanol and acetone in an ultrasonic bath (40 kHz, 120 W) for 3 × 20 min for each solvent (solvent was replaced with a fresh portion after each sonication period), dried at 120 °C for 1 h in an electric oven and then packed into a vertical air-tight column heated at 300 °C under continuous N_2 flow of ca. 30 mL min^{-1} for 1 day. $LiNTf_2$ salt was dried at 120 °C for 24 h under vacuum in a glovebox antechamber and then transferred inside the glovebox without exposure to ambient environment. 2 M $LiNTf_2$ electrolyte solution was prepared by dissolving the dried $LiNTf_2$ salt at the required concentration in dried THF using volumetric flasks inside the Ar-filled glovebox. The water content of solvents and electrolyte solutions was measured by Karl-Fisher titration with the results reported in Figure S1. Proton shuttles were dried as follows: methanol, ethanol, *n*-propanol, *iso*-propanol, *n*-pentanol, *n*-butanol were kept over activated zeolite for 5 days inside the Ar-filled glovebox; (ii) $[P_{6,6,6,1,4}][NTF_2]$ and $[P_{6,6,6,1,4}]$[eFAP] were dried using Schlenk line and then introduced to the glovebox; (iii) 0.1 M $HNTf_2$ tetrahydrofuran solution containing 2 M $LiNTf_2$ were prepared inside the glovebox and then kept over activated zeolite for at least 3 days. For experiments with low concentrations of $HNTf_2$, the dried 0.1 M $HNTf_2$ + 2 M $LiNTf_2$ solution was diluted as required.

Preparation of NH_4NTf_2 was followed the literature with modification.[2] 5 g of $HNTf_2$ was reacted with the excess of ammonia solution (250 ml) in a round bottom flask under vigorous stirring for 1 h. Then, the solution was evaporated at 80 °C under vacuum (-100 kPa) of the rota-vap (200 rpm) to obtain a white salt. This white salt was dissolved in 250 ml of ammonia solution and dried with the same, aforementioned procedure. This step was repeated twice. In the final step, the round bottom flask containing the dried salt was quickly removed from the rota-vap and immediately transferred to the antechamber attached with the Ar-filled glovebox. The salt was dried at 80 °C for 24 h before being stored in the Ar-filled glovebox. To confirm stoichiometry, the pH of a 0.1 M NH_4NTf_2 aqueous solution was measured as *ca* 6.12 using a pH meter (smartCHEM-pH).

The water content for the employed proton shuttles is summarised in Figure S1. All chemicals required for the preparation of the electrolyte solutions, as well as prepared and used electrolyte solutions, were stored inside the Ar-filled glovebox at all times. To prepare the 0.1 M water in tetrahydrofuran solution containing 2 M $LiNTf_2$, the desired amount of water (for 5 ml of electrolyte, *ca* 9 µl water is needed) was transferred into a 2 ml glass chromatographic sample vial with pre-assembled septa screw cap in the ambient air. A gentle flow of Ar gas (ca. 2 ml min^{-1}) was applied to the headspace of the vial for 1 min. After that, the vial was quickly closed and introduced to the glovebox. To mix water with 2 M $LiNTf_2$ solution, 1 ml from 5 ml electrolyte solution was rapidly added into 2 ml glass vial containing water as soon as the vial was opened, the mixture then was introduced back to the remained electrolyte solution.

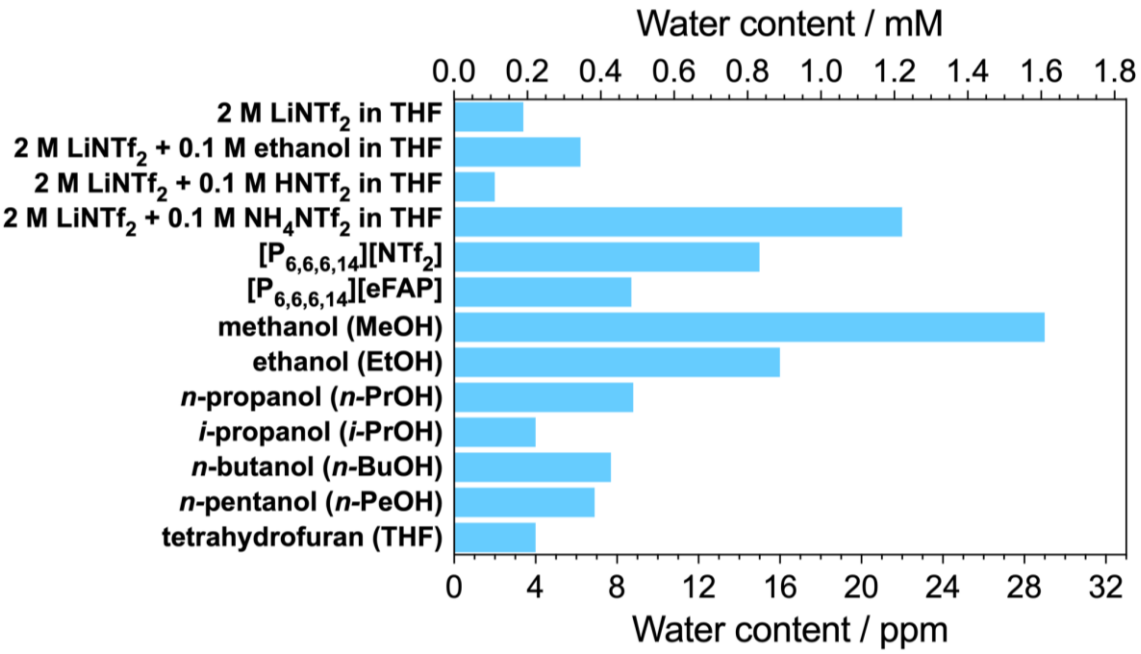

Figure S1. Water concentration in solutions and solvents employed for experiments.

Electrochemical cell employed for all NRR and control experiments was a gas-tight PEEK vessel where working and reference electrodes were located in the centre of a helical coil (*d* = 16 mm) of the auxiliary electrode, especially for single-compartment configuration (Figure S2a). To enable experiments in a two-compartment configuration, a glass tube with a ceramic P3 frit (pore size 16 - 40 µm) was used to confine the counter electrode (Figure S2b). Unless specifically mentioned, experiments were undertaken in a single-compartment configuration. The experiments always involved a fixed volume of gas.

The auxiliary electrode was a platinum wire, which was washed by ultrasonication (40 kHz, 120 W) in absolute ethanol for 1 h, dried under a flow of compressed nitrogen and then flame-annealed using a propane-butane burner. As a reference electrode, a silver wire confined within a fritted glass tube filled with the same electrolyte solution as in the main compartment was used. Prior to each experiment, the fritted tube was washed with absolute ethanol under ultrasonication (40 kHz, 120 W) for 30 min and then additionally by pushing ethanol through the frit under nitrogen gas pressure. After repeating these procedures for 3 times, the fritted tube was dried in an oven at 120 °C for 1 h and then at 80 °C under vacuum for 20 min.

The potential of the employed silver wire quasi-reference electrode was calibrated against the apparent potential of the lithium(0/+) process, which was estimated from the crossover point in cyclic voltammetry. The potential measured in this manner is not a true potential of the $Li^{0/+}$ redox couple as it is affected by the chemical reactions with N_2, proton source and possibly tetrahydrofuran under conditions employed herein. Therefore, it is referred to as an *apparent* lithium(0/+) potential throughout the paper ($Li^{0/+}_{app}$). The detailed calibration of the $Li^{0/+}_{app}$ on the ferrocene$^{0/+}$ ($Fc^{0/+}$) scale was report in our previous work.[3]

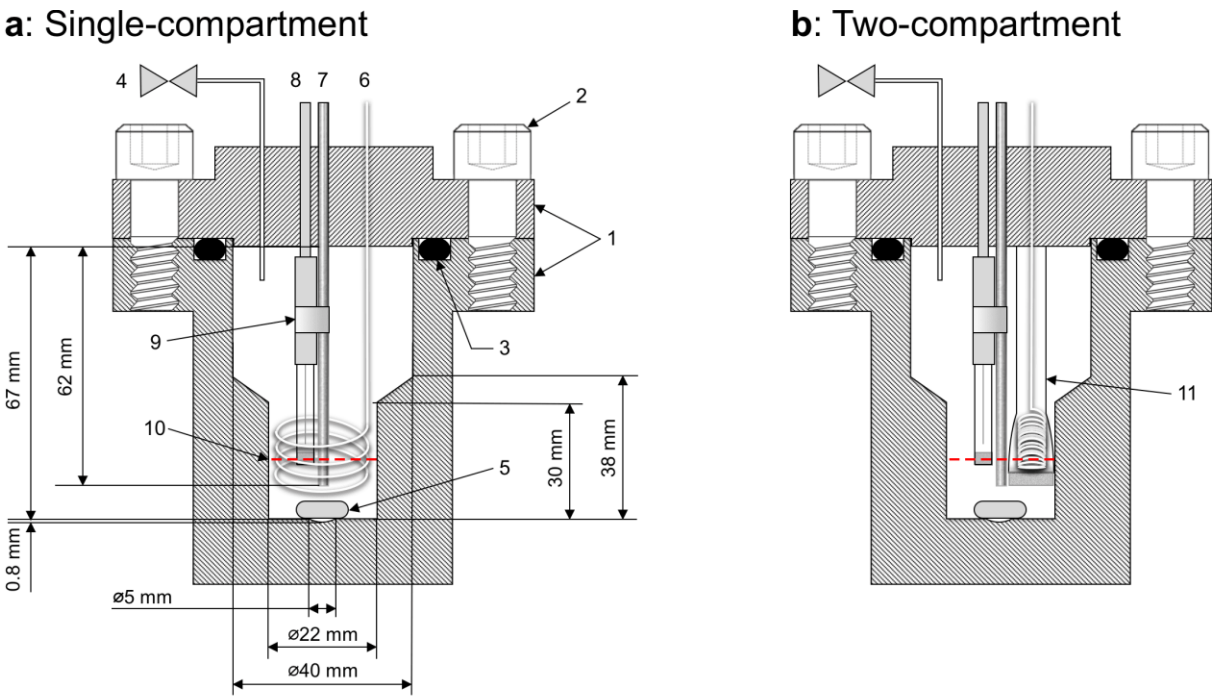

1. Cell body - polyether ether ketone
2. Hex socket cap screws
3. O-ring
4. Gas line
5. Magnetic stirring bar with dimensions of *l* = 10 mm and *d* = 3 mm
6. Platinum auxiliary electrode - Inner diameter of the helical coil is 16 mm
7. Bare nickel working electrode
8. Silver wire quasi-reference electrode confined behind a glass frit
9. Polyethylene brace - affixing working electrode to quasi-reference electrode
10. Level of the 5 ml electrolyte
11. Glass frit to separate the auxiliary electrode from the working compartment

Figure S2. Scheme of the high-pressure electrochemical cell configurations.
(a) Single-compartment and (b) two-compartment cell.

In standard preparation procedure, the cell was soaked in 0.1 M $KOH_{(aq.)}$ and then in 0.05 M $H_2SO_{4(aq.)}$ for several hours in each solution, which was followed by an intense wash with water and then absolute ethanol before introducing into the glovebox for assembly. This washing procedure has proven to be highly efficient for removal of any residual ammonia and other unwanted contaminants, including oxidised forms of nitrogen (NO_x), that might interfere with the NRR. Further, every part of the cell was dried by flushing with compressed nitrogen flow and kept in an electric oven at 120 °C for 1 h. All volumetric flasks, containers, vials and other labware used to prepare and store the solutions and chemicals were washed and dried following the same procedures as those employed for the cell. The level of NH_3/NO_x impurities in the system was determined by undertaking argon control experiments (see Figure S14) and in our previous work.[3]

After completion of the cleaning procedures, all components of the electrochemical cell along with the required labware were further kept under ultra-high vacuum at 80 °C in the glovebox antechamber for at least 15 min to remove the moisture absorbed from the laboratory. After 3 repeats of the antechamber Ar refill / evacuation cycles, the cell was finally transferred into the Ar-filled glovebox for assembly and filling of the different compartments with the electrolyte solutions as required. Upon completion of these procedures, the cell was tightly sealed and removed from the

glovebox for pressurising with either N_2 or Ar gas in a manner that excludes penetration of air into the interior of the cell. Subsequently, the system was allowed to equilibrate for *ca* 30 min while stirring the electrolyte solution in the main chamber with a Teflon-lined magnetic stirring bar having the dimensions of l = 10 mm and d = 3 mm at 600 rpm (IKA magnetic stir plate; colour squid S5). After completion of the experiment, the pressurised gas was slowly released and all yield rate and faradaic efficiency data are based on the amount of ammonia produced in the working electrolyte solution only.

Amounts of accumulated NH_3 in the working electrolyte solution was collected and quantified at the end of the electrochemical measurements, which included the following: (i) electrochemical impedance spectroscopy at a potential corresponding to the stabilised open-circuit potential value; (ii) cyclic voltammetry (20 cycles at a scan rate v = 0.020 V s^{-1}), (iii) resting (relaxing) at an open circuit while recording the potential of the working electrode (15 min), (iv) chronoamperometry at required potential for a required period of time, (v) resting at an open circuit while recording the potential of the working electrode (15 min), and (vi) cyclic voltammetry (v = 0.020 V s^{-1}; 20 cycles). Importantly, comparisons of the voltammograms measured in steps (ii) and (vi) provided a measure of the shift of the potential of the Ag wire quasi-reference electrode during the chronoamperometric step (iv).

All key experiments were reproduced at least three times (Table S1) and the corresponding data are presented in the main text as mean ± one standard deviation. Generally the standard deviations obtained were greater than the individual analysis C.I's (*vide infra*).

Ammonia/ammonium analysis

Due to high amounts of ammonia produced in the experiments, dilution of the samples of the electrolyte solutions with water by a factor of 10-2000 was required. To ensure reliable quantification, application of at least two significantly different dilutions to the same sample is highly recommended; this strategy was employed herein for most of the key experiments.

Spectrophotometric Berthelot analysis[4, 5] was employed for the routine quantification of ammonia. To this end, 500 µl of the sample was added to a 2 ml Axygen microtube and mixed with 400 µl of 1 M $NaOH_{(aq.)}$ containing 5 wt.% salicylic acid and 5 wt.% tri-sodium citrate. This was followed by the sequential addition of 100 µl of 0.05 M $NaClO_{(aq.)}$ and 30 µl of 1 wt.% sodium nitroprusside aqueous solution. The resulting homogeneous mixture was incubated in the dark at ambient temperature for exactly 2 h and then immediately transferred into a polystyrol/polystyrene 10 mm cuvette (Sarstedt) for recording a UV-vis spectra (Cary spectrophotometer) within a 500-1000 nm range at a scan rate of 10 nm s^{-1}. Background spectra were recorded for each sample using Berthelot's reagents solution in water for the analysis of the electrolyte. All absorbance data are reported after correction for the background values.

Reliable quantitative Berthelot analysis of the electrolysed tetrahydrofuran solutions could not be achieved using a regular calibration plot approach, and required the implementation of the method of standard additions to account for the interfering effects of the environment specific to each sample. In a typical procedure, 1 ml of the diluted sample was added into six Axygen microtubes (2 ml), to which 1 mL of either 0, or 10, or 20, or 30, or 40 or 50 µM NH_4Cl in H_2O was added (Figure S3). The resulting 6 mixtures were further analysed following the standard Berthelot

spectrophotometric method described above. Plots of the absorbance at 655 nm *vs.* concentration of added NH_4Cl were fitted with a linear dependence, which X-intercept was divided by the slope to obtain the ammonia concentration in the analysed diluted sample.[1, 6]

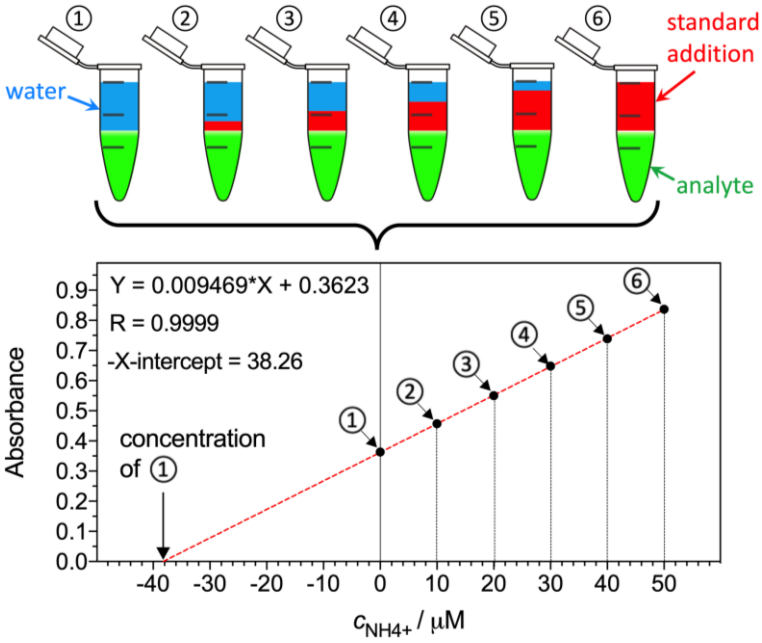

Figure S3. Quantification of ammonium using the method of standard additions applied to spectrophotometric Berthelot analysis.

In this example, the concentration of ammonia in the analysed sample of the 2 M $LiNTf_2$ + 0.1 M C_2H_5OH tetrahydrofuran solution after the Li-NRR test (diluted by a factor 4000) was 0.3623/ 0.00947 = 38 (C.I. ± 0.4) µM (precision indicated is calculated from the statistical analysis for the 95% confidence level).[6] Absorbance data are presented after the background correction.

Physical characterisation

X-ray photoelectron spectroscopic (XPS) analysis was performed using a Nexsa Surface Analysis System, ThermoFisher Scientific instrument with a monochromatic Al K_α source (1486.6 eV). X-ray spot size was set to 400 µm × 800 µm. The analysis chamber was maintained at a pressure of 1.0×10^{-8} mbar or less. Survey scans were recorded at a pass energy of 200 eV and a step size of 1 eV, while high resolution data were obtained at a pass energy of 50 eV and a step size of 0.1 eV. Samples were loaded onto the holder inside the Ar-filled glovebox and left under vacuum in the glovebox antechamber for 10 min before being transported to the instrument without contacting ambient environment at any stage. The samples were kept in ultra-high vacuum overnight before XPS measurements were carried out. No electrical contact between the sample and the instrument ground was present, and the samples were charge neutralised before the analysis. Depth profiling was undertaken using an Ar^+ ion source operated at 500 eV, scanned over 2 mm x 2 mm area with a sequence of 600 and 1200 seconds. The estimated sputtering rate is *ca.* 0.08 nm s^{-1}. Collected spectral data were energy corrected by adjusting the maximum of the aliphatic C-C peak in C 1s spectra to 284.8 eV. Data processing was performed by using Avantage software with version 5.9902.

UV-Vis spectroscopic analysis of electrolyte solutions was performed using Agilent Cary 60 UV-Vis spectrophotometer equipped with a xenon source lamp. The solutions were dropped on a quartz cuvette, which has 10 µm path length and 250 nL capacity. The solution droplet was required a certain time to be absorbed inside the cuvette by capillary depending on the viscosity of the solution. Between measurements, the cuvette was immersed inside acetone for 1 h, then dried in vacuum oven for 15 min. The measurement was recorded within 190 – 1100 nm range at scan rate of 300 nm min^{-1}.
NMR analysis of the electrolyte solutions were recorded using Bruker Avance III 400 NMR spectrometer with a 9.4 T magnet and 5 mm BBFO probe (^{1}H at 400.130 MHz; ^{13}C at 100.613 MHz and ^{19}F at 376.498 MHz) at a controlled temperature of 25 °C.
Electrolyte solution samples were analysed directly, without further dilution by taking 0.6 mL of the post reaction mixture and placing it in an NMR tube. A sealed capillary containing d_6-benzene was used for sample locking as well as chemical shift (δ / ppm) referencing. A total of 32 transients with a recycle delay of 1 s were collected for ^{1}H spectra; 2000 transients with a recycle delay of 3 s were collected for ^{13}C spectra, 2000 transients with a recycle delay of 2 s were collected for ^{13}C DEPTQ135 spectra and 80 transients with a recycle delay of 1 s were collected for ^{19}F spectra. Carbon multiplicity of the side product was determined using a DEPTQ135 experiment.

2. EXTENDED ELECTROCHEMICAL AND Li-NRR DATA

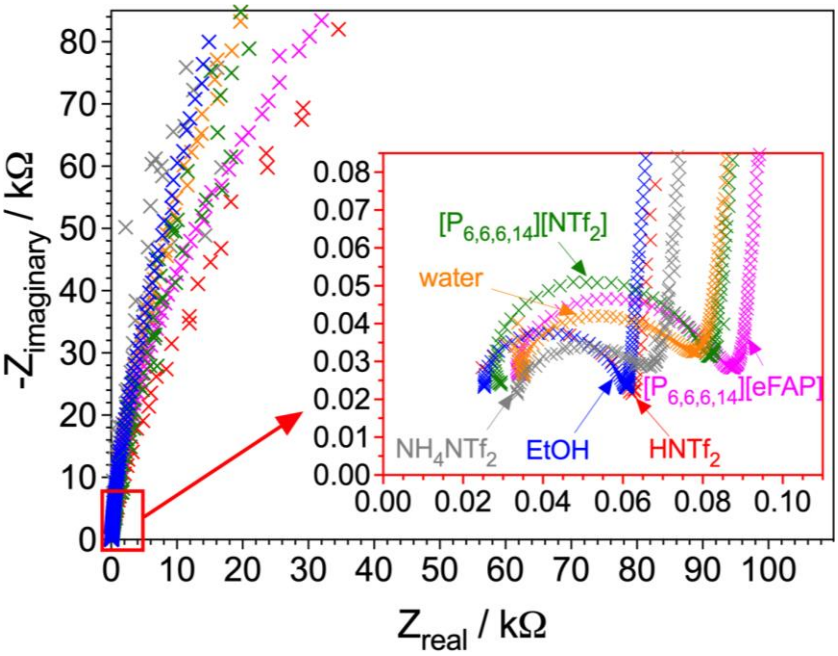

Figure S4. Resistance of 2 M $LiNTf_2$ solutions with different proton carriers.
Electrochemical impedance spectroscopy (EIS) of a bare nickel wire (0.15 cm^2) in N_2-saturated (15 bar) 2 M $LiNTf_2$ tetrahydrofuran solutions containing 0.1 M C_2H_5OH (*blue*), $[P_{6,6,6,14}][eFAP]$ (*magenta*), $[P_{6,6,6,14}][NTf_2]$ (*green*), $HNTf_2$ (*red*), water (*orange*) and NH_4NTf_2 (*grey*). No stirring was applied during the measurements. The higher resistance minimum is assigned to the resistance of the electrolyte in the cell.

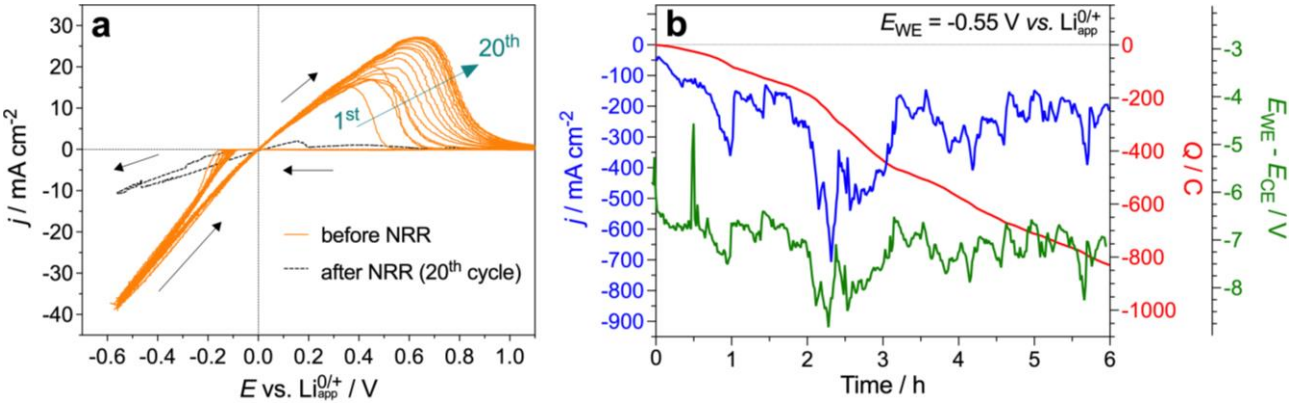

Figure S5. Electrochemical data for the Li-NRR with 0.1 M H_2O.
(a) Cyclic voltammetry (0.020 V s^{-1}; 20th scan; arrows show the sweep direction) before (*orange*; *teal arrows* show the evolution of the oxidation peak from 1st to 20th cycle) and after the Li-NRR (*black* dashed curve), (b) evolution of current density (*blue*), cell potential (*green*) and charge passed (*red*) during chronoamperometric tests in 2 M $LiNTf_2$ tetrahydrofuran solution containing 0.1 M water at -0.55 V *vs.* $Li^{0/+}_{app}$. Horizontal dashed lines show (a, b) j = 0 mA cm^{-2} and (b) Q = 0 C, while the vertical dashed line shows E = 0 V *vs.* $Li^{0/+}_{app}$. Solutions were continuously stirred during voltammetry and chronoamperometry.

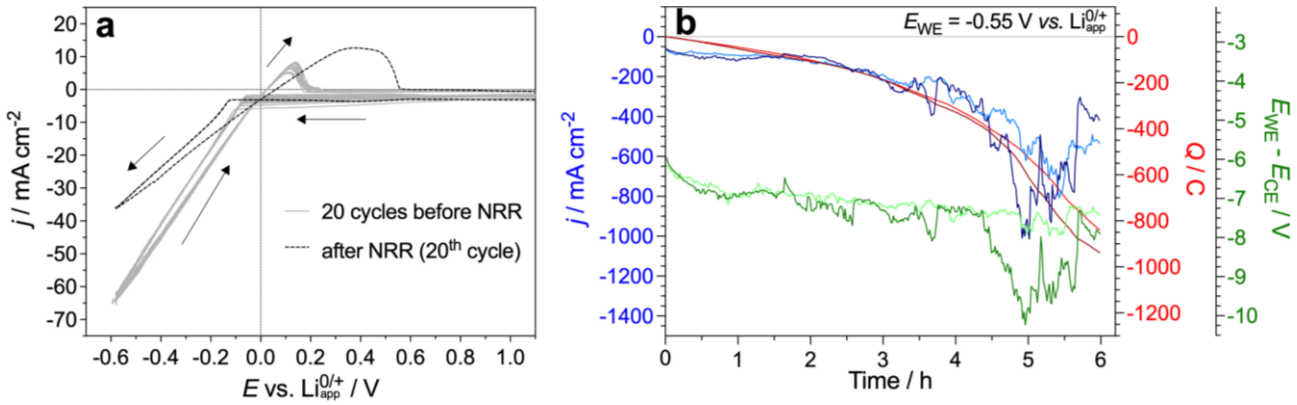

Figure S6. Electrochemical data for the Li-NRR with 0.1 M NH_4NTf_2.

(a) Cyclic voltammetry (0.020 V s^{-1}; 20th scan; arrows show the sweep direction) before (*grey*) and after the Li-NRR (*black* dashed curve), (b) evolution of current density (*blue*), cell potential (*green*) and charge passed (*red*) during chronoamperometric tests in 2 M $LiNTf_2$ tetrahydrofuran solution containing 0.1 M NH_4NTf_2 at -0.55 V *vs.* $Li^{0/+}_{app}$. Horizontal dashed lines show (a, b) j = 0 mA cm^{-2} and (b) Q = 0 C, while the vertical dashed line shows E = 0 V *vs.* $Li^{0/+}_{app}$. Solutions were continuously stirred during voltammetry and chronoamperometry.

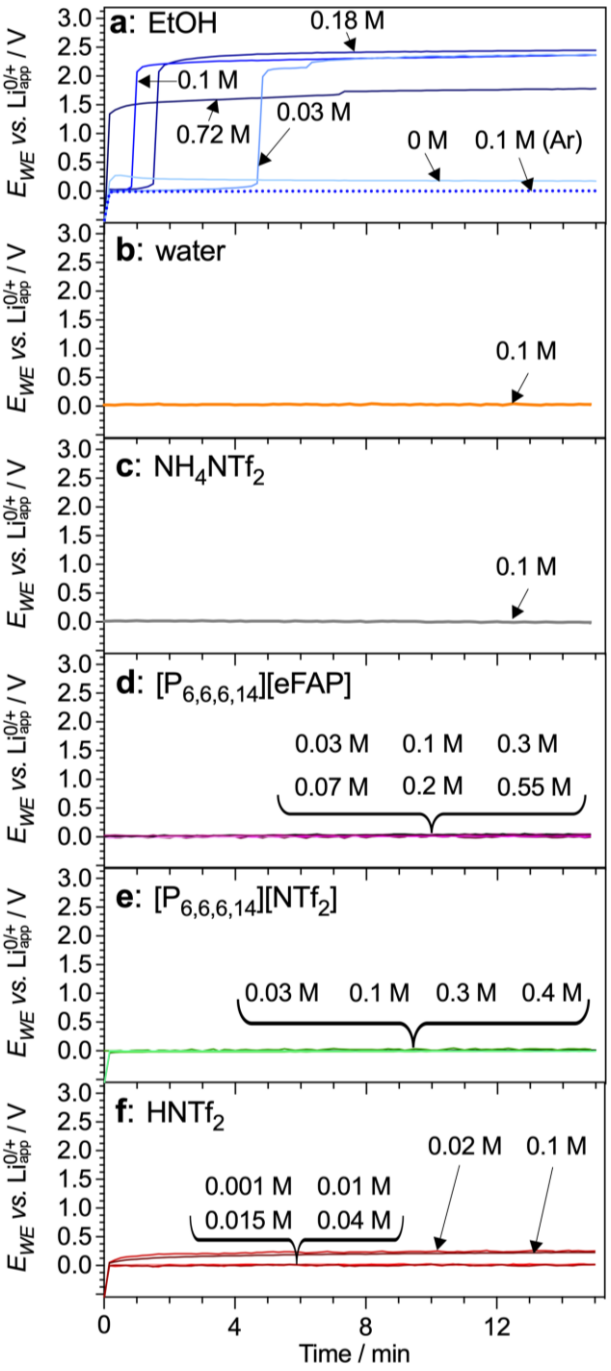

Figure S7. Relaxation of the working electrode potential after the Li-NRR.

Measurements were undertaken under open circuit conditions upon completion of the chronoamperometric experiments with 2 M $LiNTf_2$ shown in Figure 1b (main text) and Figure S5-6 and 8 using different proton carriers: (a) none (*light blue*) and varied concentrations of EtOH (*tints of blue*; see figure); (b) 0.1 M water; (c) 0.1 M NH_4NTf_2 ; (d) varied concentrations of $[P_{6,6,6,14}][eFAP]$ (*tints of magenta;* see figure); (e) varied concentrations of $[P_{6,6,6,14}][NTf_2]$ (*tints of green*; see figure); (f) varied concentrations of $HNTf_2$ (*tints of red*; see figure). Panel a additionally shows data obtained under 15 bar Ar (*dotted*). Other conditions as in Figure 1 and Figure S5.

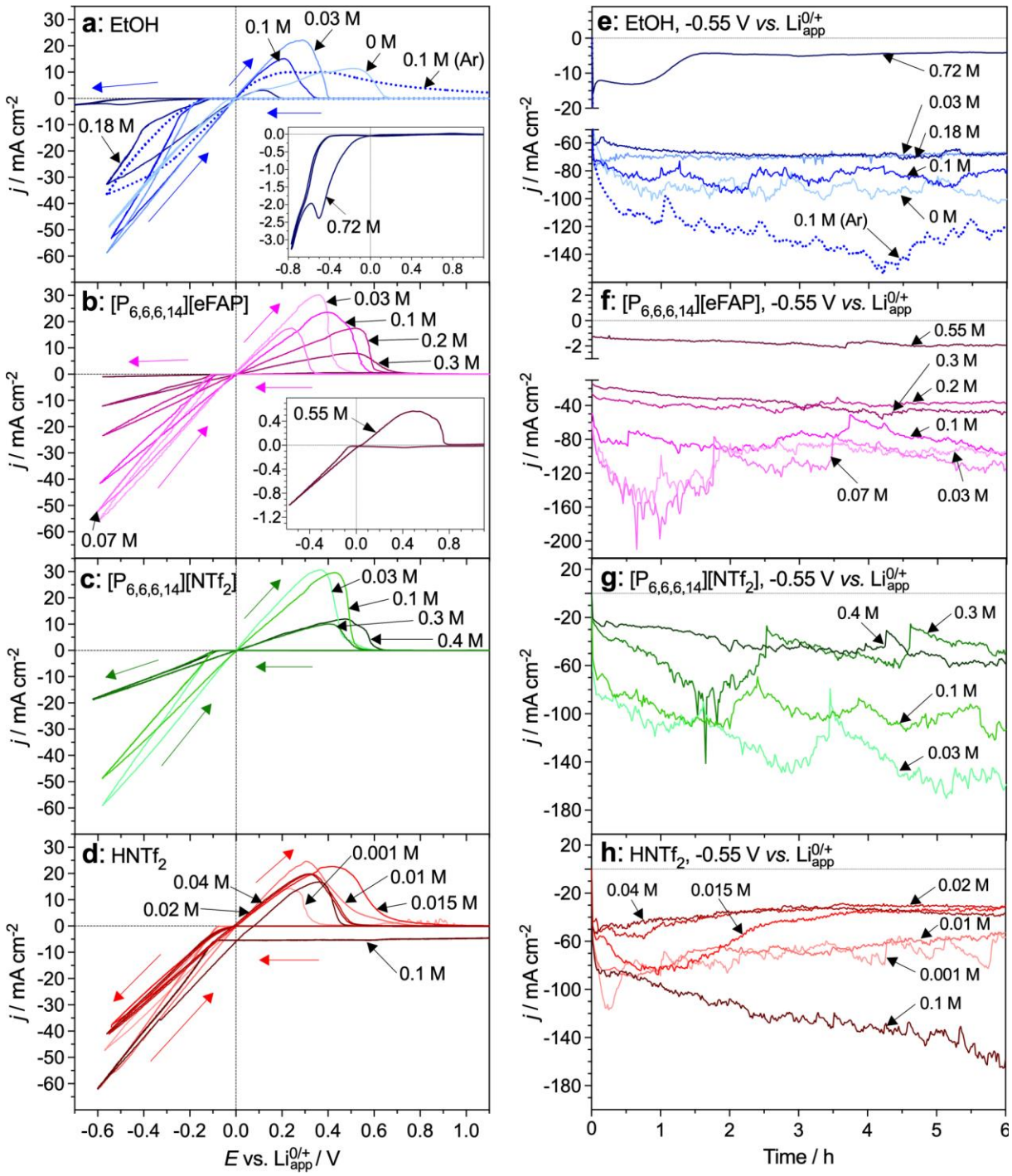

Figure S8. Electrochemical data for the Li-NRR with different proton carriers.

(a-d) Effects of the proton carrier on the initial cyclic voltammetry (0.020 V s^{-1}; 20th scans; arrows show sweep direction; inset shows enhanced plot for 0.72 M ethanol; vertical and horizontal dashed lines show E = 0 V *vs.* $Li^{0/+}_{app}$ and j = 0 mA cm^{-2}), (e-h) and evolution of the current density during chronoamperometric tests at -0.55 V *vs.* $Li^{0/+}_{app}$ (horizontal dashed line shows j = 0 mA cm^{-2}). Experiments were undertaken under 15 bar N_2 (static atmosphere) in continuous stirred 2 M $LiNTf_2$ tetrahydrofuran solution with the following proton carriers: (a, e) none (*light blue*) and varied concentrations of EtOH (see figure); (b, f) varied concentrations of $[P_{6,6,6,14}][eFAP]$ (*tints of magenta;* see figure); (c, g) varied concentrations of $[P_{6,6,6,14}][NTf_2]$ (*tints of green*; see figure), and (d, h) varied concentrations of $HNTf_2$ (*tints of red*; see figure). Panels a and e additionally show data obtained under 15 bar Ar (*dotted*).

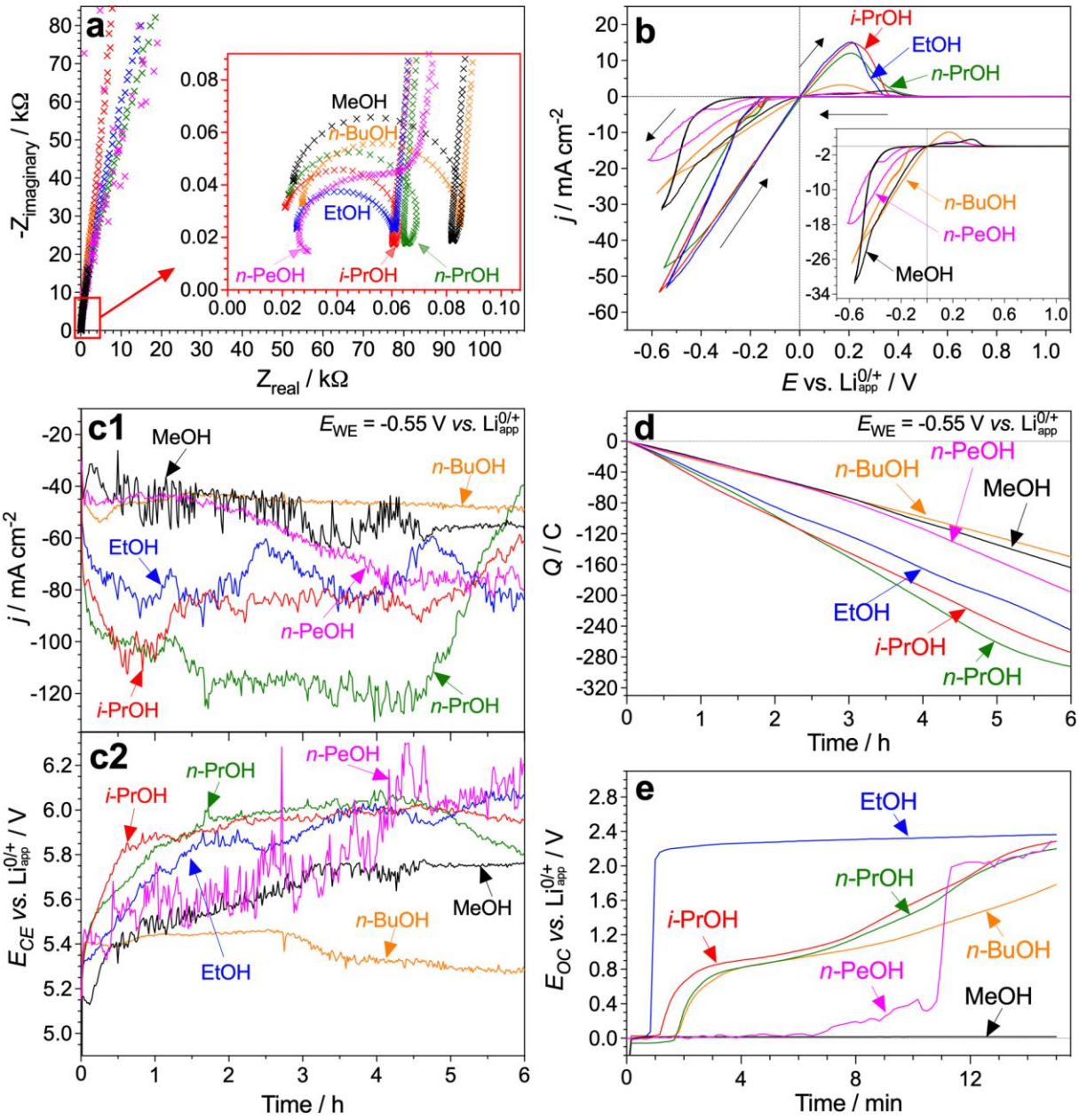

Figure S9. Electrochemical data for the Li-NRR with different alcohols.

Effects of the alcohol proton carrier (all present at 0.1 M) on the (a) initial EIS (insets show enhanced plots of the semi-circles for all alcohols), (b) initial cyclic voltammetry (0.020 V s^{-1}; 20th scans; inset shows enhanced plot for *n*-butanol and methanol; vertical and horizontal dashed lines show E = 0 V *vs.* $Li^{0/+}_{app}$ and j = 0 mA cm^{-2}), (c) evolution of the current density and (d) auxiliary electrode potential during chronoamperometric tests at -0.55 V *vs.* $Li^{0/+}_{app}$. Experiments were carried out under 15 bar N_2 (static atmosphere) using different proton carriers: methanol (*black*), ethanol (*blue*), *n*-propanol (*green*), *i*-propanol (*red*), *n*-butanol (*orange*) and *n*-pentanol (*magenta*). Solutions were not stirred during EIS, and continuously stirred during voltammetry and chronoamperometry. Other conditions as in Figure S5.

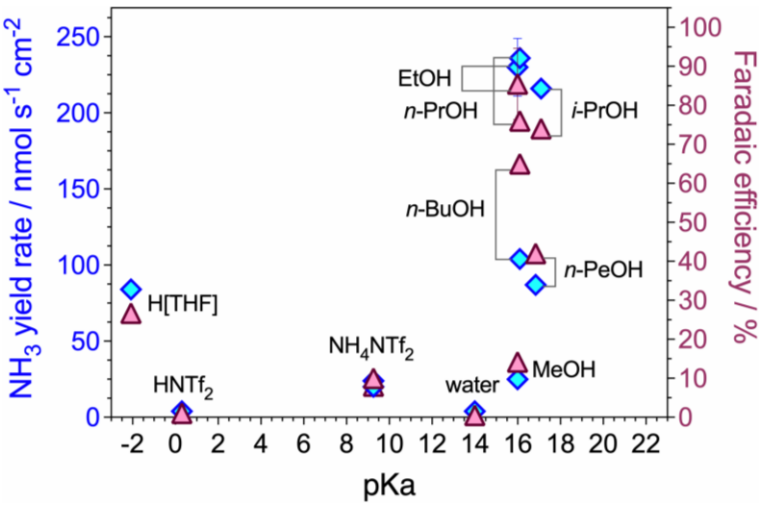

Figure S10. Li-NRR metrics *vs.* pKa value of the proton carrier.
Ammonia yield rate (*diamonds*) and the Li-NRR faradaic efficiency (*triangles*) plotted against pKa value of the proton source added[7-12] at 0.1 M concentration (except for the tetrahydrofuran data, which represent a solution with no intentionally added proton source). Experiments were undertaken in a single-compartment cell -0.55 V *vs.* $Li^{0/+}_{app}$ using a bare Ni wire electrode (0.15 cm^2) and stirred tetrahydrofuran solutions containing the corresponding proton source along with 2 M $Li[NTf_2]$ and saturated with N_2 at 15 bar (static atmosphere). Data for ethanol show mean and one standard deviation derived from multiple repeats of the experiment (Table S1). pKa value of $[P_{6,6,6,14}]^+$ based ionic liquids is unavailable and pKa value of protonated tetrahydrofuran is unreliable.

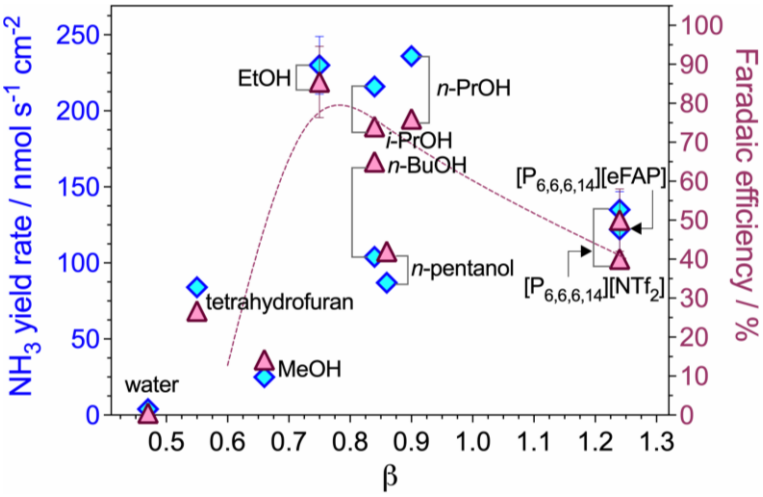

Figure S11. Li-NRR metrics *vs.* Kamlet-Taft *β* parameter of the proton carrier.
Ammonia yield rate (*diamonds*) and the Li-NRR faradaic efficiency (*triangles*) plotted against Kamlet-Taft hydrogen bond accepting parameter (*β*) of the proton source added at 0.1 M concentration (except for the tetrahydrofuran data, which represent a solution with no intentionally added proton source). Experiments were undertaken in a single-compartment cell -0.55 V *vs.* $Li^{0/+}_{app}$ using a bare Ni wire electrode (0.15 cm^2) and stirred tetrahydrofuran solutions containing the corresponding proton source along with 2 M $LiNTf_2$ and saturated with N_2 at 15 bar (static atmosphere). Data for EtOH show mean and one standard deviation derived from multiple repeats of the experiment (Table S1).

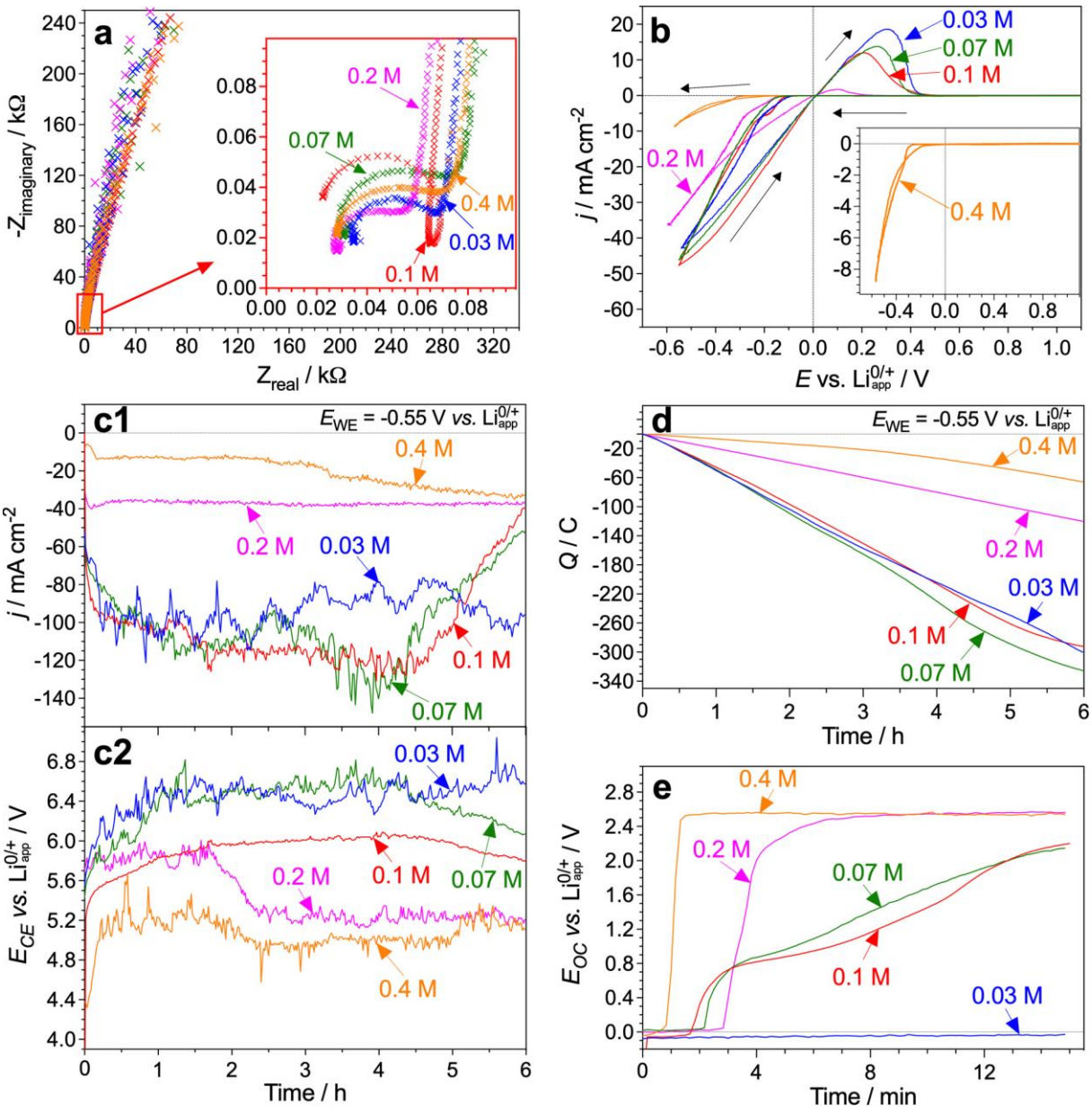

Figure S12. Electrochemical data for the Li-NRR with *n*-PrOH.

(a) Electrochemical impedance spectroscopy measured at open circuit potential (insets show enhanced plots of the semi-circles for all concentrations), (b) cyclic voltammetry (0.020 V s^{-1}; 20th scan; arrows show the sweep direction), evolution of (c) the current density and the auxiliary electrode potential, (d) charge passed during chronoamperometric tests at -0.55 V *vs.* $Li^{0/+}_{app}$, and (e) subsequent evolution of the working electrode open circuit potential recorded for a bare nickel wire electrode (0.15 cm^2) in 2 M $LiNTf_2$ along with 0.03 (*blue*), 0.07 (*green*), 0.1 (*red*), 0.2 (*magenta*) and 0.4 M (*orange*) *n*-PrOH. Horizontal dashed lines show (b-c) j = 0 mA cm^{-2} and (d) Q = 0 C, while the vertical dashed line shows E = 0 V *vs.* $Li^{0/+}_{app}$. Solutions were not stirred during EIS, and continuously stirred during voltammetry and chronoamperometry. Other conditions as in Figure S5.

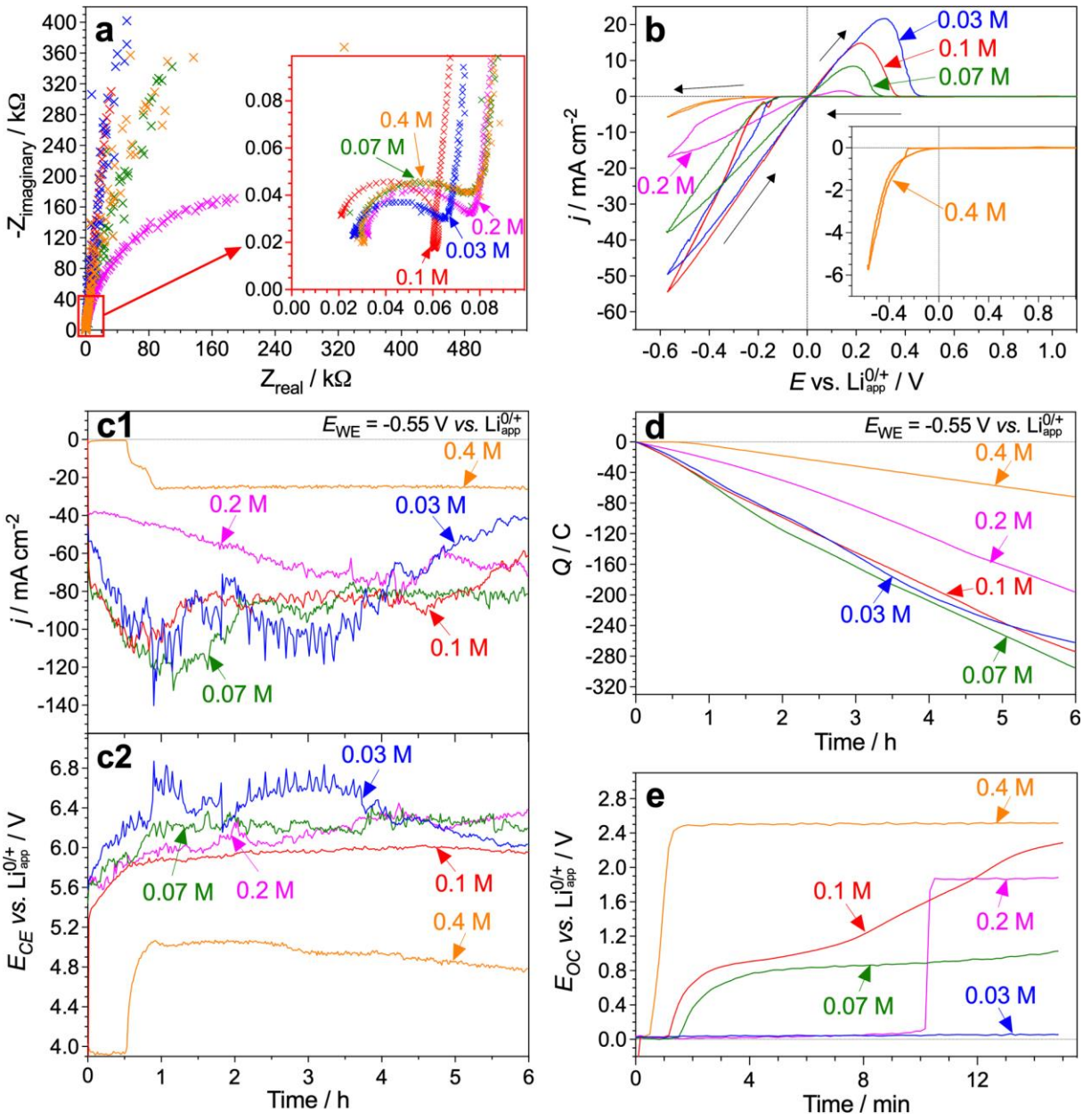

Figure S13. Electrochemical data for the Li-NRR with *i*-PrOH.

(a) Electrochemical impedance spectroscopy measured at open circuit potential (insets show enhanced plots of the semi-circles for all concentrations), (b) cyclic voltammetry (0.020 V s^{-1}; 20th scan; arrows show the sweep direction), evolution of (c) the current density and the auxiliary electrode potential, (d) charge passed during chronoamperometric tests at -0.55 V *vs.* $Li^{0/+}_{app}$, and (e) subsequent evolution of the working electrode open circuit potential recorded for a bare nickel wire electrode (0.15 cm^2) in 2 M Li[NTf_2] along with 0.03 (*blue*), 0.07 (*green*), 0.1 (*red*), 0.2 (*magenta*) and 0.4 M (*orange*) *i*-PrOH. Horizontal dashed lines show (b-c) j = 0 mA cm^{-2} and (d) Q = 0 C, while the vertical dashed line shows E = 0 V *vs.* $Li^{0/+}_{app}$. Solutions were not stirred during EIS, and continuously stirred during voltammetry and chronoamperometry. Other conditions as in Figure S5.

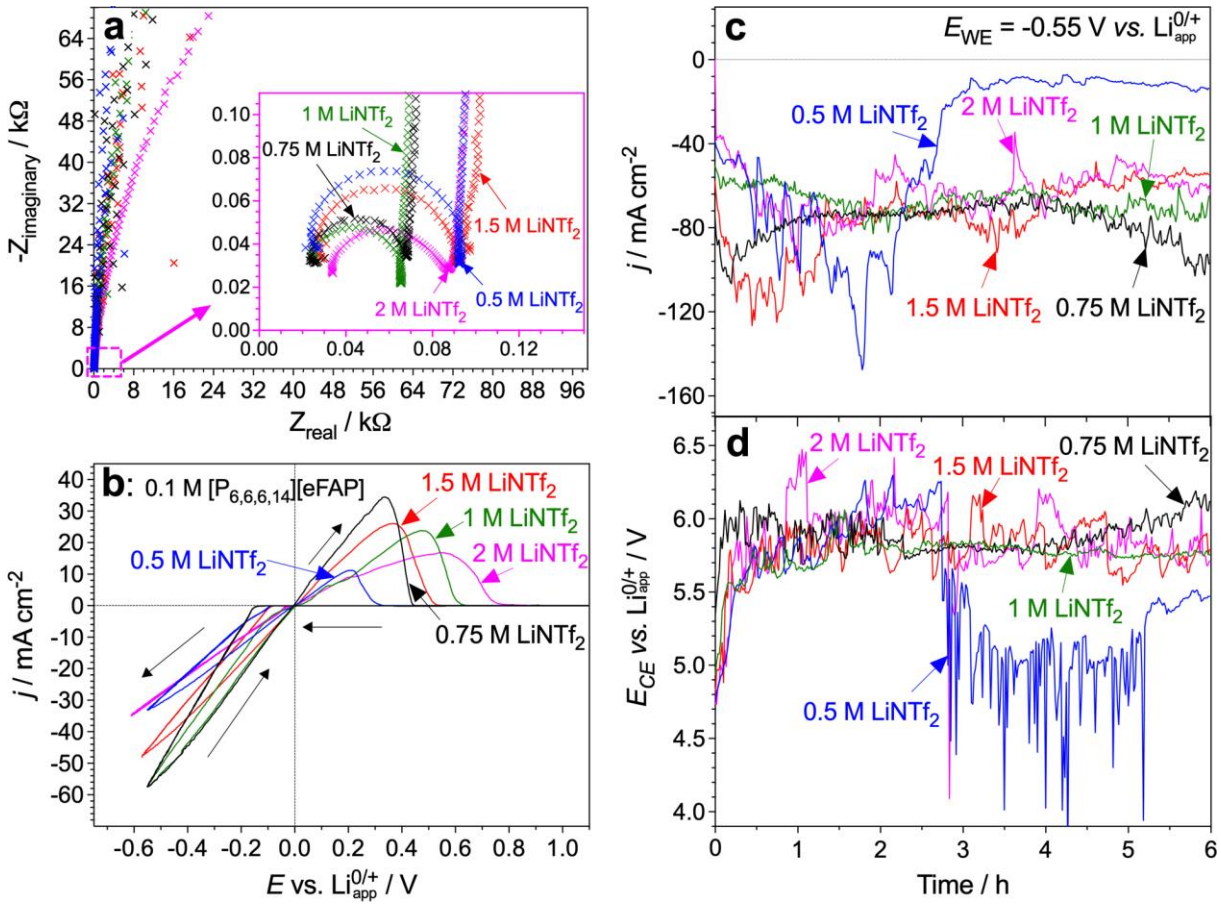

Figure S14. Electrochemical data for the Li-NRR with 0.1 M [$P_{6,6,6,14}$][eFAP] and different $LiNTf_2$ concentrations.

(a) Electrochemical impedance spectroscopy measured at open circuit potential (insets show enhanced plots of the semi-circles for all concentrations), (b) cyclic voltammetry (0.020 V s^{-1}; 20th scan; arrows show the sweep direction), evolution of (c) the current density and (d) the auxiliary electrode potential during chronoamperometric tests at -0.55 V *vs.* $Li^{0/+}_{app}$ recorded for a bare nickel wire electrode (0.15 cm^2) in 0.5 (*blue*), 0.75 (*black*), 1 (*green*), 1.5 (*red*) and 2 M (*magenta*) $LiNTf_2$ along with 0.1 M [$P_{6,6,6,14}$][eFAP]. Horizontal dashed lines show (b-c) j = 0 mA cm^{-2}, while the vertical dashed line shows E = 0 V *vs.* $Li^{0/+}_{app}$. Solutions were not stirred during EIS, and continuously stirred during voltammetry and chronoamperometry. Other conditions as in Figure S5.

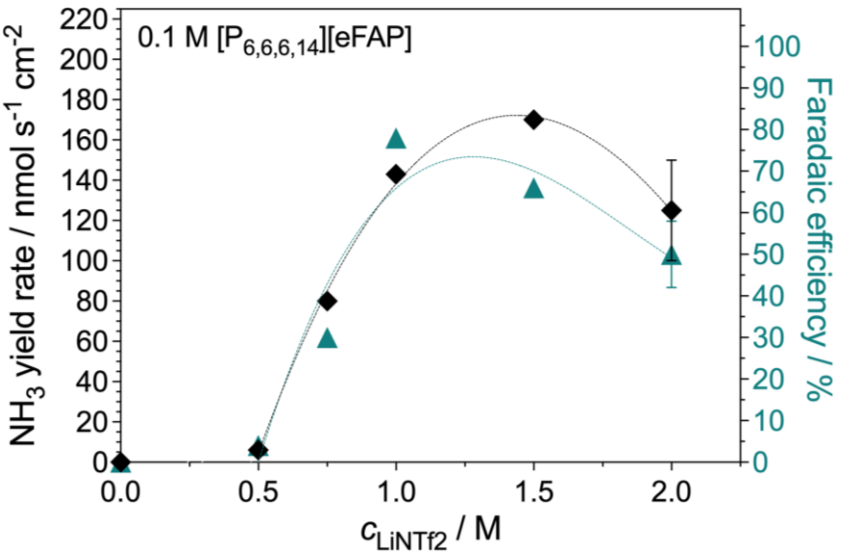

Figure S15. $LiNTf_2$ concentration effects on the Li-NRR with $[P_{6,6,6,14}]^+$.

Effects of the $LiNTf_2$ concentration on the ammonia yield rate (*black diamonds*) and NRR faradaic efficiency (*teal triangles*) for 0.1 M $[P_{6,6,6,14}]$[eFAP] proton shuttle. Experiments were undertaken in a single-compartment cell -0.55 V *vs.* $Li^{0/+}_{app}$ using a bare Ni wire electrode (0.15 cm^2) and stirred tetrahydrofuran solutions containing corresponding concentration of $LiNTf_2$ and saturated with N_2 at 15 bar (static atmosphere). Data with error bars show mean and one standard deviation derived from more than three independent repeats of the same experiment (Table S2). Three repeats at 1 M $LiNTf_2$ had standard deviation smaller than the points.

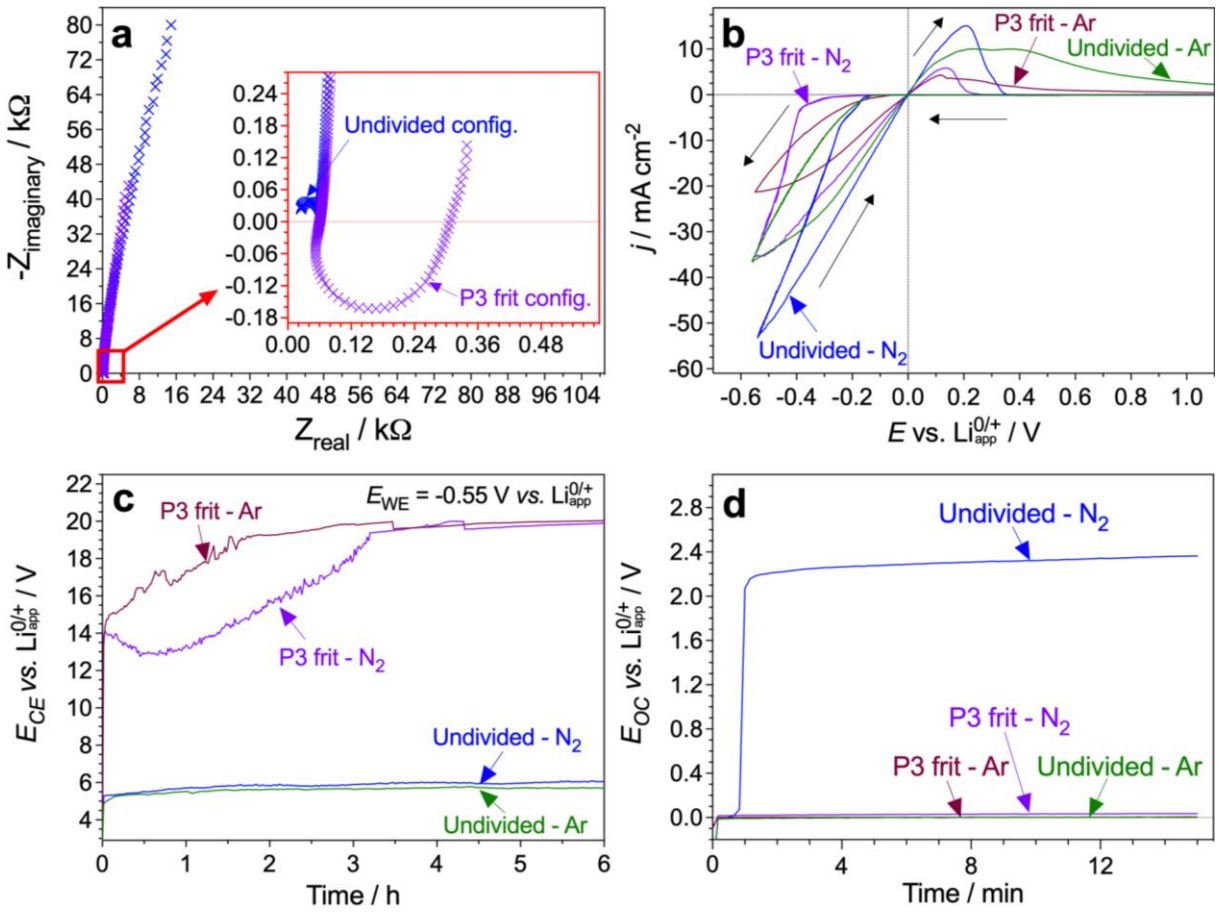

Figure S16. Electrochemical behaviour in single- and two-compartment cell configurations. Comparisons of the electrochemical data obtained without (*blue*, *green*) and with (*purple*, *wine*) a P3 ceramic frit separating the working and auxiliary electrodes: (a) electrochemical impedance spectroscopy (insets show enhanced plots of the semi-circles), (b) cyclic voltammetry (0.020 V s^{-1}; 20th scan; arrows show scan direction; vertical and horizontal dashed lines show E = 0 V *vs.* $Li^{0/+}_{app}$ and j = 0 mA cm^{-2}), (c) evolution of the auxiliary electrode potential during chronoamperometric reduction at -0.55 V *vs.* $Li^{0/+}_{app}$ and (d) subsequent evolution of the working electrode open circuit potential. Experiments were undertaken using a bare nickel wire electrode (0.15 cm^2) in 2 M $LiNTf_2$ + 0.1 M EtOH tetrahydrofuran solutions saturated with Ar (*green*, *wine*) or N_2 (*blue*, *purple*) at 15 bar. The working electrolyte solution was continuously stirred during voltammetric and chronoamperometric measurements.

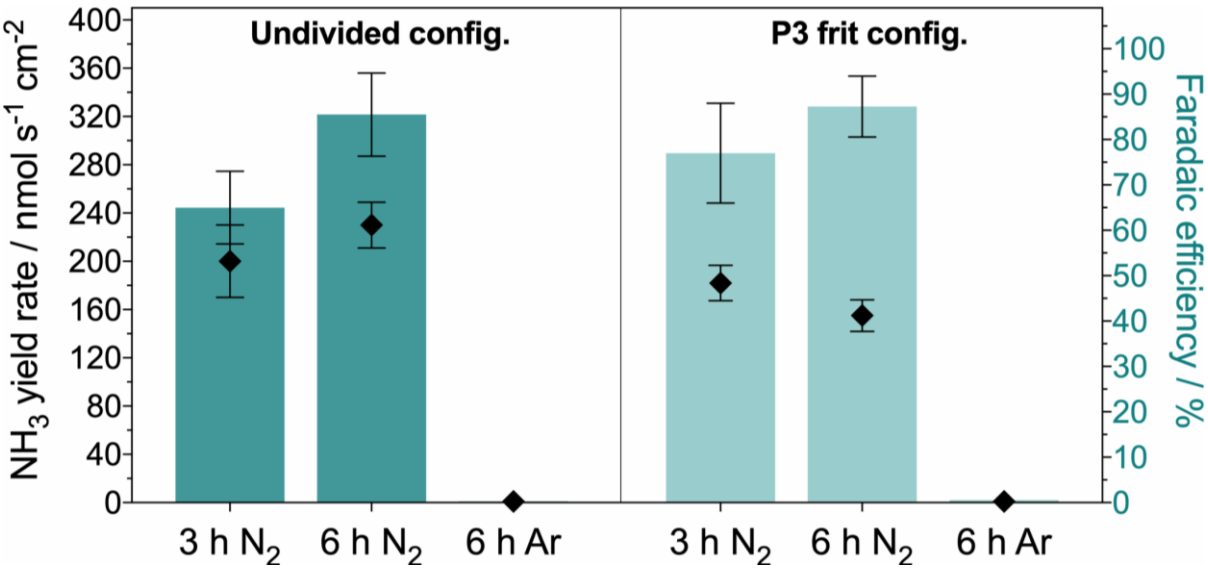

Figure S17. Li-NRR metrics in single- and two-compartment cell configurations.
Ammonia yield rate (*diamonds*) and faradaic efficiency (*bars*) measured after 3 and 6 h chronoamperometric experiments at -0.55 V *vs.* $Li^{0/+}_{app}$ in a single- (left) and two-compartment (right) cell configuration. Other experimental details as in Figure S16. Data are shown as a mean and one standard deviation derived from multiple repeats of each experiment.

3. EFFECTS OF THE PROTON CARRIER CONCENTRATION

Dependencies of the ammonia yield-rate and the Li-NRR faradaic efficiency on the concentration of EtOH, *n*-PrOH and *i*-PrOH were very similar (Figure S18). Importantly, maximal values of the Li-NRR performance metrics were achieved at the same value of the proton carrier concentration, suggesting that the major electrochemically-induced transformations in the system are indeed the proton and nitrogen reduction reactions, which compete with each other. Moreover, the optimal concentration values were apparently the same for the three alcohols examined, *viz.* close to 0.1 M, which additionally confirms that they are similarly effective proton carriers for the Li-mediated NRR under conditions relevant to Figure S18.

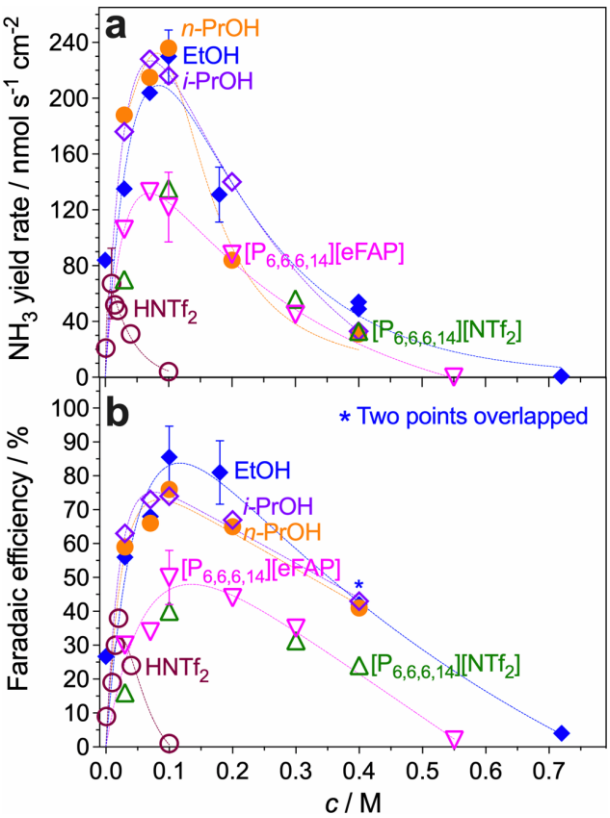

Figure S18. Proton source effects on the Li-mediated NRR.
Effects of the concentration of EtOH, *n*-PrOH, *i*-PrOH, $HNTf_2$, $[P_{6,6,6,14}][eFAP]$ and $[P_{6,6,6,14}][NTf_2]$ on the (a) ammonia yield rate and (b) NRR faradaic efficiency. Experiments were undertaken in a single-compartment cell -0.55 V *vs.* $Li^{0/+}_{app}$ using a bare Ni wire electrode (0.15 cm^2) and stirred tetrahydrofuran solutions containing 2 M $LiNTf_2$ and saturated with N_2 at 15 bar (static atmosphere). Data with error bars show mean and one standard deviation derived from more than three independent repeats of the same experiment (Table S1).

As discussed in the main text, 0.1 M $HNTf_2$ – a strong Brønsted acid – produced very low amounts of ammonia due to a very high activity of H^+, its reduction outrunning the Li-NRR under these conditions. However, the use of lower concentrations of $HNTf_2$, in particular 0.01 M, enabled an appreciable ammonia yield rate of 70 ± 30 nmol s^{-1} cm^{-2}. Although this value is notably lower than that provided by the 0.1 M EtOH benchmark (230 ± 20 nmol s^{-1} cm^{-2}), it is among the highest reported so far.[1, 13-16] However, the faradaic efficiency of the process was as low as 19 ± 1 % with

0.01 M $HNTf_2$, which could be improved to *ca* 40% when using 0.02 M $HNTf_2$ but at the expense of the ammonia yield rate (Figure S18b and Table S1). This dependence differs to that recorded for alcohols in the sense that the highest FE and yield rate are achieved at different proton source concentrations. Possibly, the excessive acidity of $HNTf_2$ and thereby very weak basicity of NTf_2^- cannot provide the intricate balance of the proton transport between the working and auxiliary electrodes and kinetics of the chemical and electrochemical processes occurring in the system in the optimal manner under the conditions examined herein. This is partially corroborated by the very long (>15 min) relaxation of the working electrode potential after chronoamperometric tests with $HNTf_2$ irrespective of its concentration (Figure S7f), indicating presence of the very significant amounts of reduced products on the cathode that cannot be rapidly removed by reaction even with a strongly acidic $HNTf_2$. However, a more significant disbalancing factor is likely the consumption of a significant portion of charge on the degradation of the electrolyte solution components and resulting growth of crude deposits on the electrode surface (Figure S21). Although further improvements in the performance might emerge through optimisations of the mass-transport regime in the system and even more precise tuning of the $HNTf_2$ concentration, the resulting system is likely to be highly unstable due to the very high sensitivity of the Li-NRR on the amount of this proton carrier present (Figure S18). Nevertheless, the use of bis(trifluoromethane)sulfonimide as a proton shuttle in the $LiNTf_2$-mediated NRR system might be a promising approach due to its high electrochemical stability and chemical simplification of the system, which would only contain a single $[NTf_2]^-$ anion.

Dependence of the performance of the N_2 reduction mediated by 2 M $LiNTf_2$ on the concentrations of $[P_{6,6,6,14}][eFAP]$ and $[P_{6,6,6,14}][NTf_2]$ was the same within experimental error, confirming the lack of significant effects of the anion, with the maximal FE again achieved at 0.1 M (Figure S18b). The highest NH_3 yield rate was provided by a similar yet still lower concentration of the phosphonium cation (Figure S18a), which we again ascribe to the contributions from the additional degradation processes resulting in the formation of a deposit on the electrode surface (Supplementary Figures 23-24). Thus, optimisation of the $[P_{6,6,6,14}]^+$ concentration with 2 M $LiNTf_2$ electrolyte could not provide significant improvements in the Li-NRR performance.

In summary, the Li-NRR faradaic efficiency and ammonia yield rate achieve their maxima at some optimal concentrations of proton carrier, which are very close to each other for the high-performance systems like EtOH, *n*-PrOH, *i*-PrOH and phosphonium cation. The best results, however, emerge from the optimisation of the concentration of all key components, *viz.* lithium electrolyte, proton shuttle and also concentration (partial pressure) of N_2. The effects of the latter on the Li-NRR with 2 M $LiNTf_2$ and 0.1 M EtOH as well as with 0.1 M $LiBF_4$ and 0.1 M $[P_{6,6,6,14}][eFAP]$ are discussed elsewhere.[1, 3]

4. ELECTROCHEMICALLY INDUCED TRASFORMATIONS WITHIN THE SYSTEM

Working electrode surface

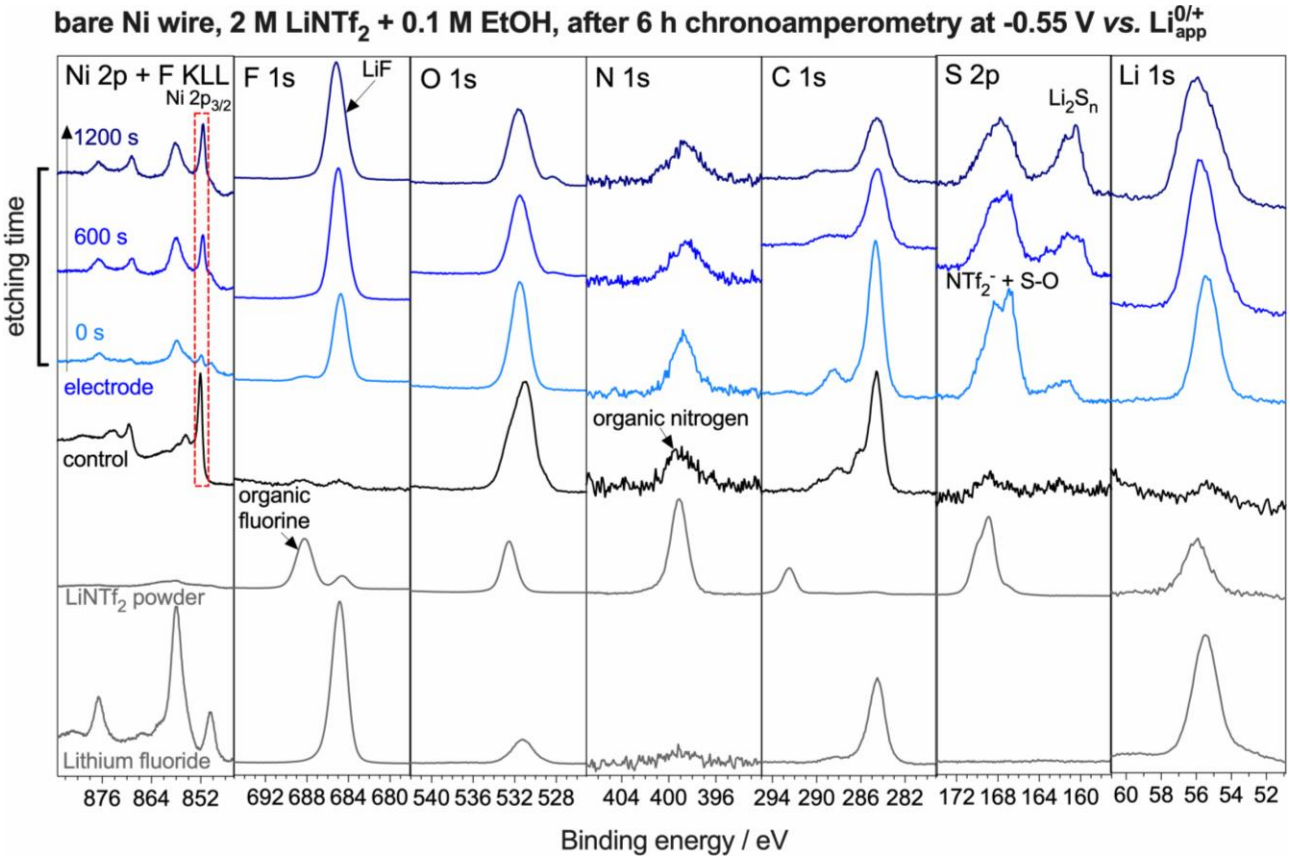

Figure S19. XPS analysis of the Ni electrode after the Li-NRR with 0.1 M EtOH.

X-ray photoelectron spectra of the surface collected in the completely immersed area of the bare nickel wire electrode in the 2 M $LiNTf_2$ + 0.1 M EtOH tetrahydrofuran electrolyte solution. These data were collected for the electrode used in the Li-NRR experiment at -0.55 V *vs.* $Li^{0/+}_{app}$ in a single-compartment as those presented in the main text Figure 1d. Depth profiling of the electrode surface was achieved with different ion etching times from 0 to 1200 s (*tints of blue*, see figure). XP spectra recorded for a freshly polished nickel wire electrode that was kept in 2 M $LiNTf_2$ + 0.1 M EtOH tetrahydrofuran solution for 6 h under 15 bar N_2 are shown for comparison as *black* traces; data for $LiNTf_2$ powder and LiF powder are shown as *grey* curves. The signals of Ni $2p_{3/2}$ (*red* dash box) separated from F KLL Auger signals were clearly detected on the electrode surface after the Li-NRR.

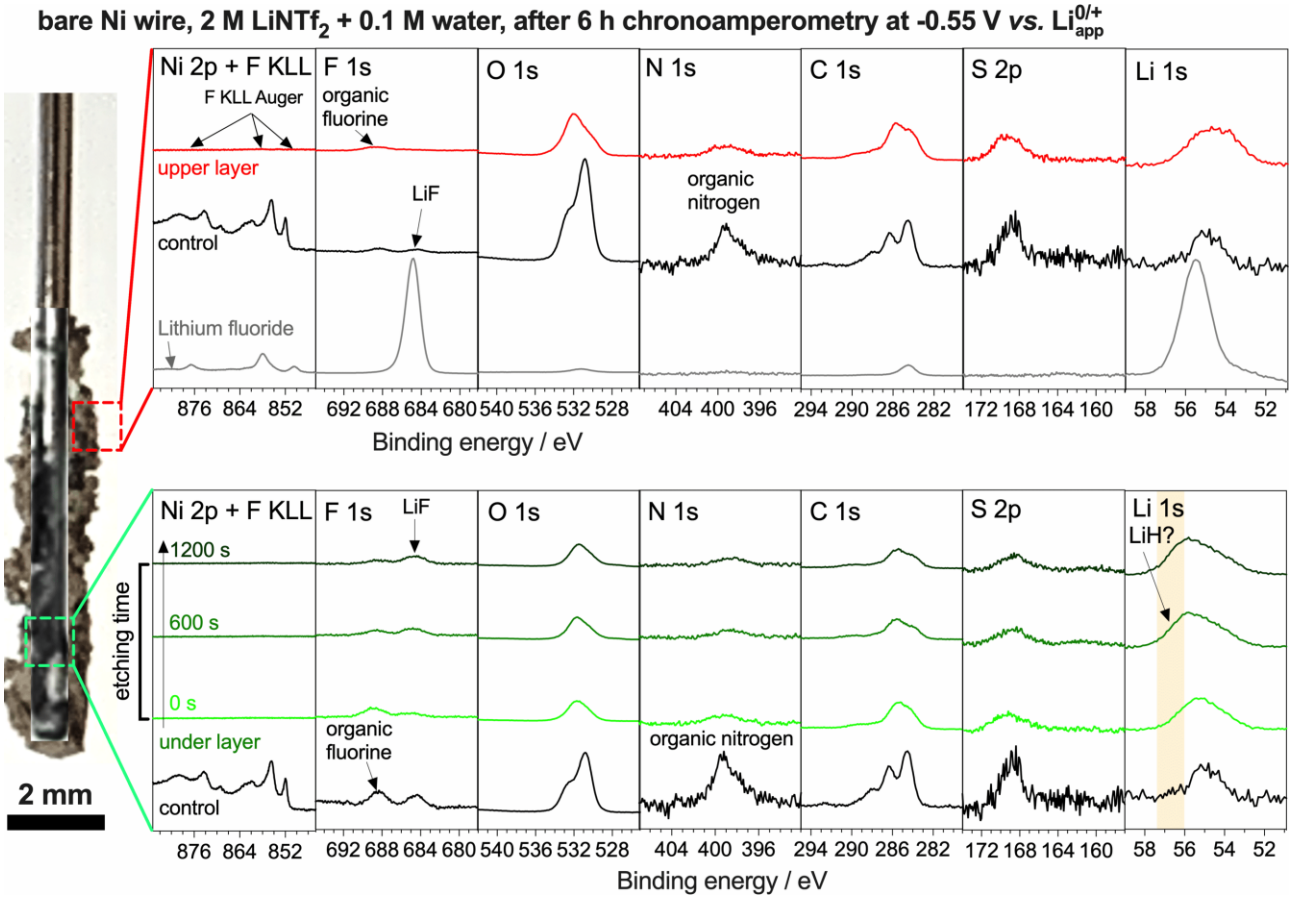

Figure S20. XPS analysis of the Ni electrode after the Li-NRR with 0.1 M H_2O.

Photographs and X-ray photoelectron spectra of the deposit (unmodified electrode; *red*) and of the near-electrode surface (after the deposit was gently removed; *green*) collected in the completely immersed area of the bare nickel wire electrode in the 2 M $LiNTf_2$ + 0.1 M water tetrahydrofuran electrolyte solution. These data were collected for the electrode used in the Li-NRR experiment at -0.55 V *vs.* $Li^{0/+}_{app}$ in a single-compartment as those presented in the main text Figure 1d. The depth profiling on the near-electrode surface was achieved with different ion etching times from 0 to 1200 s (*tints of green*, see figure). XP spectra recorded for a freshly polished nickel wire electrode that was kept in 2 M $LiNTf_2$ + 0.1 M water tetrahydrofuran solution for 6 h under 15 bar N_2 are shown for comparison as *black* traces; data for LiF powder are shown as *grey* curves. F KLL Auger signals manifest in the same binding energy range as Ni 2p. Emergence of additional signal(s) at lower binding energies (*yellow* region) in the Li 1s spectra might be attributed to the formation of lithium hydride.[17]

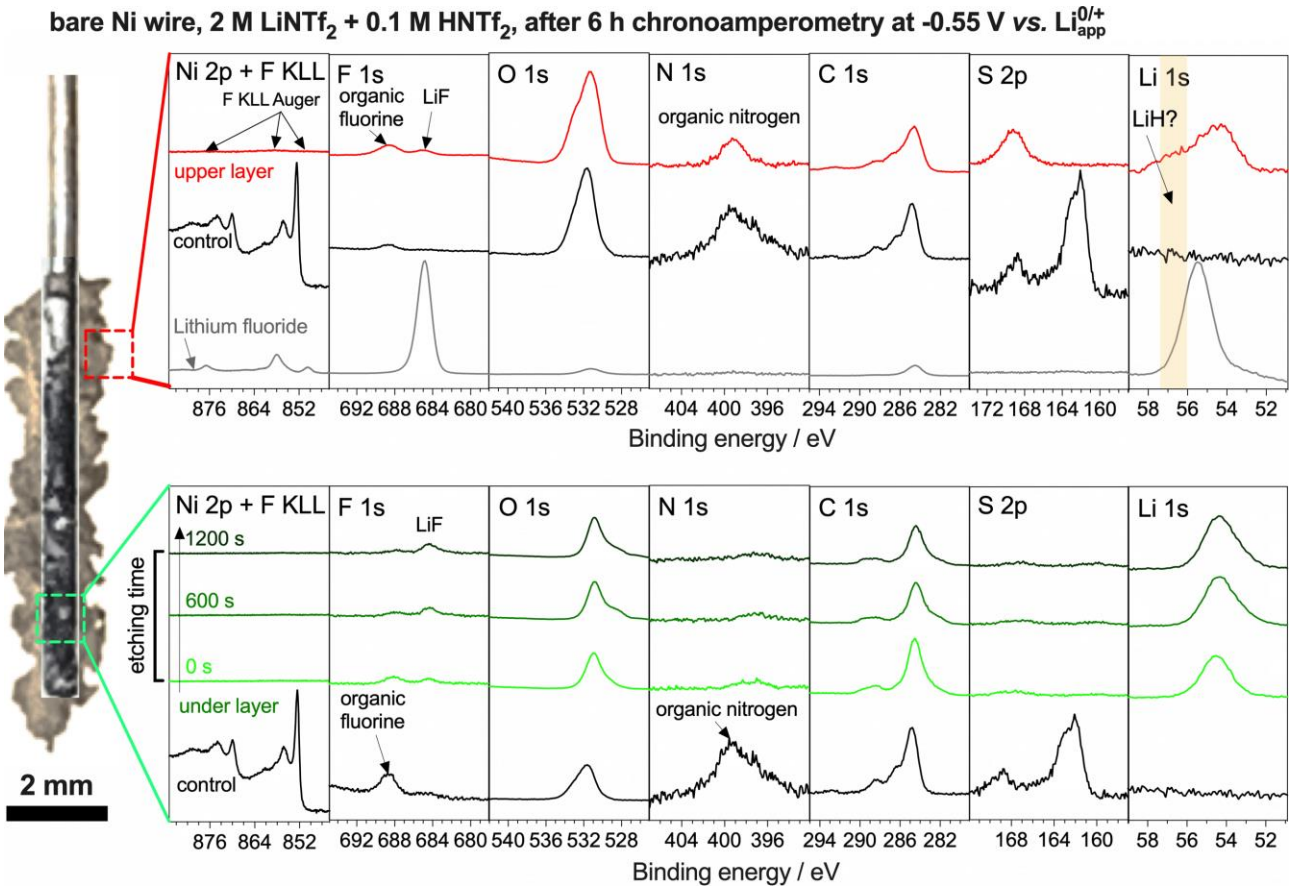

Figure S21. XPS analysis of the Ni electrode after the Li-NRR with 0.1 M $HNTf_2$.

Photographs and X-ray photoelectron spectra of the deposit (unmodified electrode; *red*) and of the near-electrode surface (after the deposit was gently removed; *green*) collected in the completely immersed area of the bare nickel wire electrode in the 2 M $LiNTf_2$ + 0.1 M $HNTf_2$ tetrahydrofuran electrolyte solution. These data were collected for the electrode used in the Li-NRR experiment at -0.55 V *vs.* $Li^{0/+}_{app}$ in a single-compartment as those presented in the main text Figure 1d. The depth profiling on the near-electrode surface was achieved with different ion etching times from 0 to 1200 s (*tints of green*, see figure). XP spectra recorded for a freshly polished nickel wire electrode that was kept in 2 M $LiNTf_2$ + 0.1 M $HNTf_2$ tetrahydrofuran solution for 6 h under 15 bar N_2 are shown for comparison as *black* traces; data for LiF powder are shown as *grey* curves. F KLL Auger signals manifest in the same binding energy range as Ni 2p. Emergence of additional signal(s) at lower binding energies (*yellow* region) in the Li 1s spectra might be attributed to the formation of lithium hydride.[17]

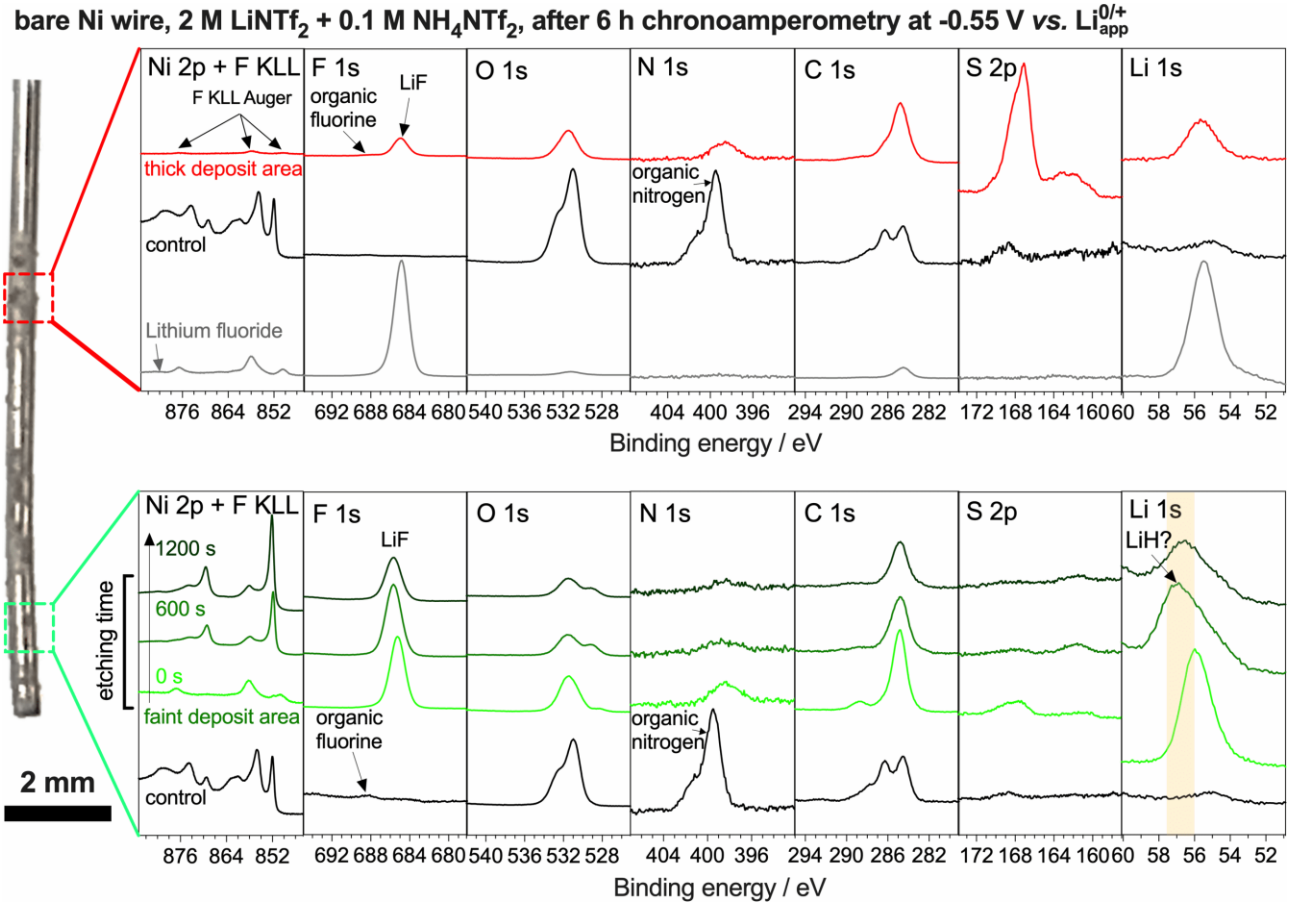

Figure S22. XPS analysis of the Ni electrode after the Li-NRR with 0.1 M NH_4NTf_2.
Photographs and X-ray photoelectron spectra of the thick (unmodified electrode; *red*) and of the faint deposit (unmodified electrode; *green*) regions collected in the completely immersed area of the bare nickel wire electrode in the 2 M $LiNTf_2$ + 0.1 M NH_4NTf_2 tetrahydrofuran electrolyte solution. These data were collected for the electrode used in the Li-NRR experiment at -0.55 V *vs.* $Li^{0/+}_{app}$ in a single-compartment as those presented in the main text Figure 1d. The depth profiling on the near-electrode surface was achieved with different ion etching times from 0 to 1200 s (*tints of green*, see figure). XP spectra recorded for a freshly polished nickel wire electrode that was kept in 2 M $LiNTf_2$ + 0.1 M NH_4NTf_2 tetrahydrofuran solution for 6 h under 15 bar N_2 are shown for comparison as *black* traces; data for LiF powder are shown as *grey* curves. F KLL Auger signals manifest in the same binding energy range as Ni 2p. Emergence of additional signal(s) at lower binding energies (*yellow* region) in the Li 1s spectra might be attributed to the formation of lithium hydride.[17]

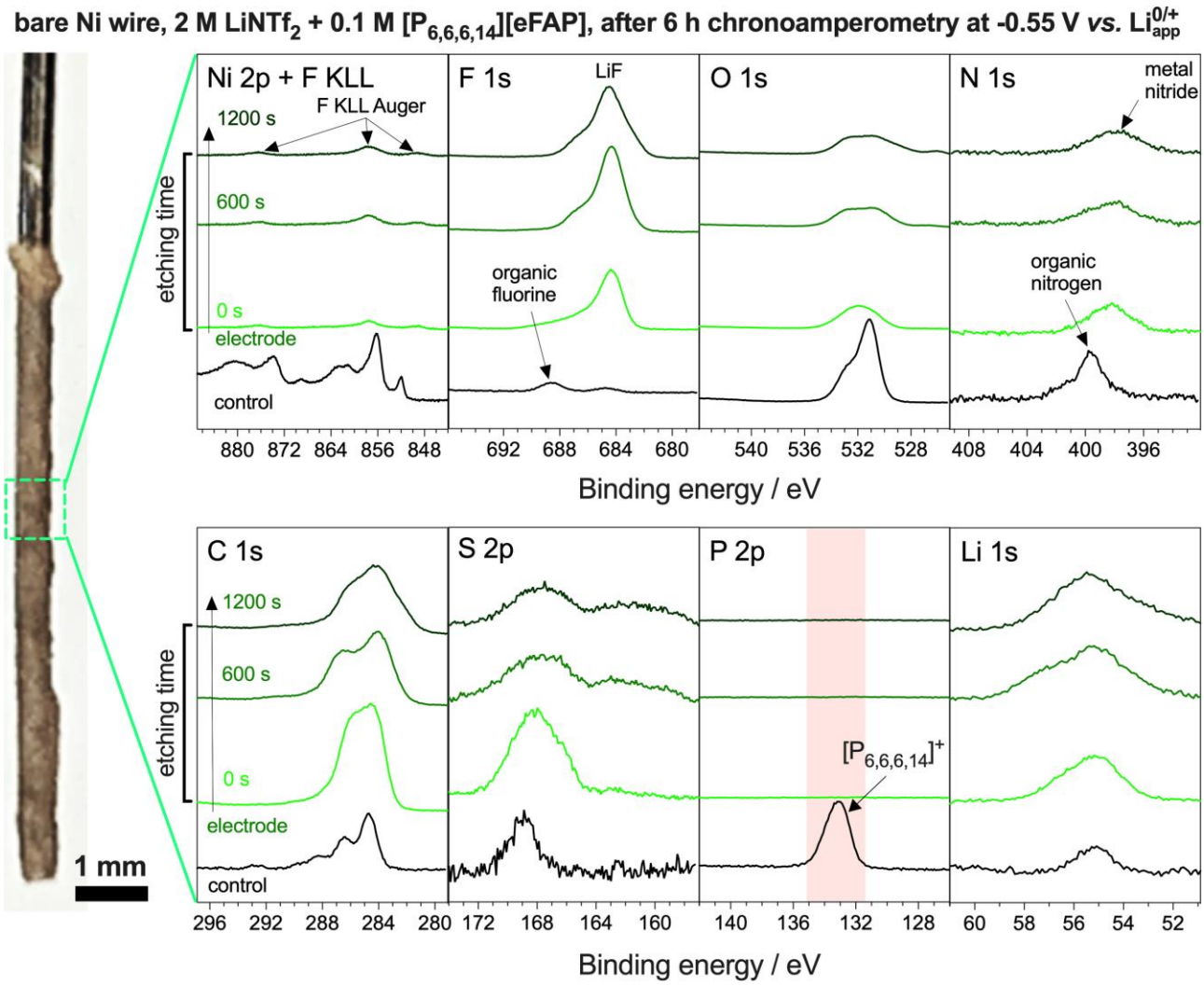

Figure S23. XPS analysis of the Ni electrode after the Li-NRR with 0.1 M [$P_{6,6,6,14}$][eFAP]. Photographs and X-ray photoelectron spectra of the deposit surface (unmodified electrode; *green*) collected in the completely immersed area of the bare nickel wire electrode in the 2 M $LiNTf_2$ + 0.1 M [$P_{6,6,6,14}$][eFAP] tetrahydrofuran electrolyte solution. These data were collected for the electrode used in the Li-NRR experiment at -0.55 V *vs.* $Li^{0/+}_{app}$ in a single-compartment as those presented in the main text Figure 1d. Depth profiling for the deposit surface was achieved with different ion etching times from 0 to 1200 s (*tints of green*, see figure). XP spectra recorded for a freshly polished nickel wire electrode that was kept in 2 M $LiNTf_2$ + 0.1 M [$P_{6,6,6,14}$][eFAP] tetrahydrofuran solution for 6 h under 15 bar N_2 are shown for comparison as *black* traces. F KLL Auger signals manifest in the same binding energy range as Ni 2p. *Red* region indicates $[P_{6,6,6,14}]^+$ signal.

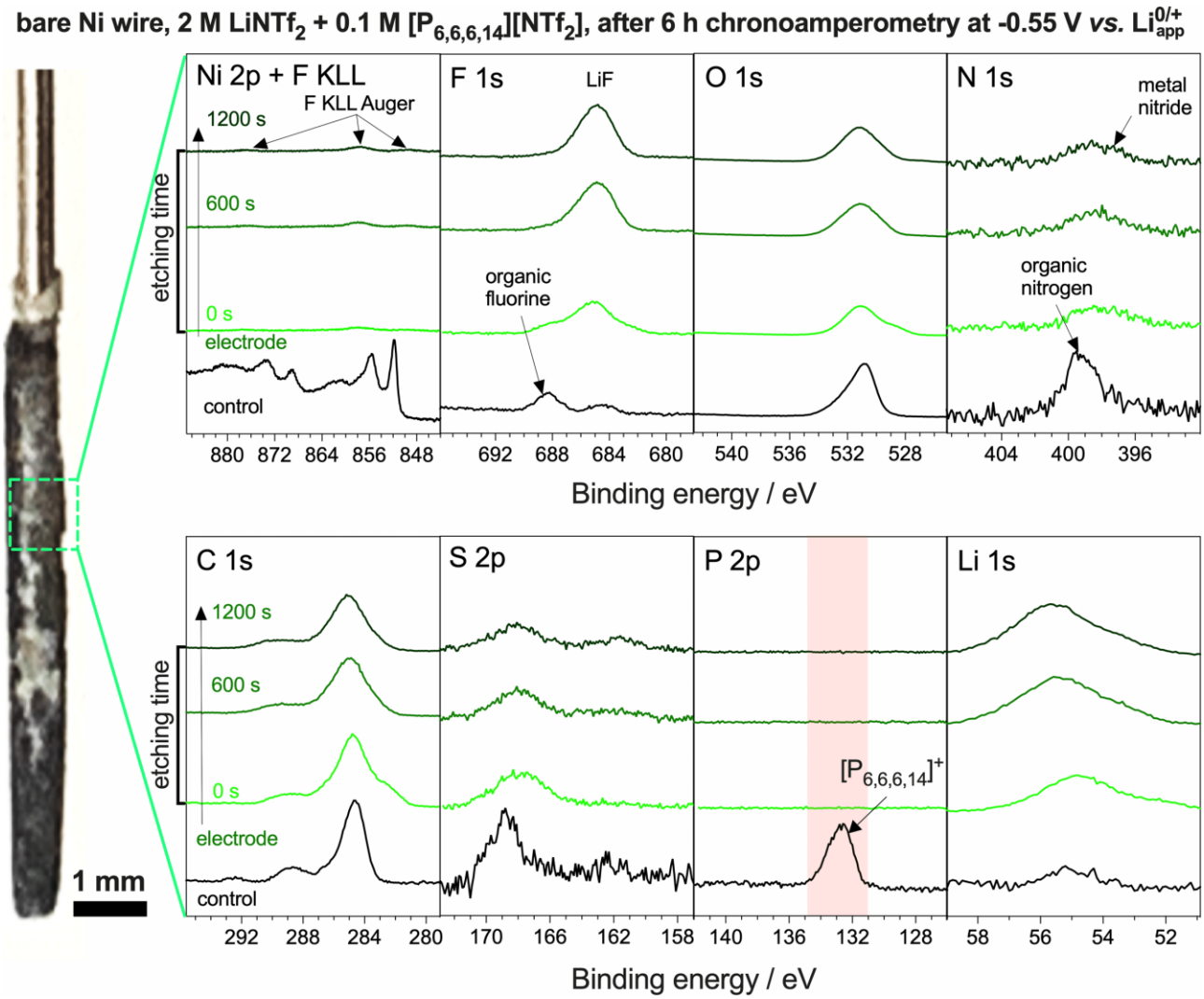

Figure S24. XPS analysis of the Ni electrode after the Li-NRR with 0.1 M $[P_{6,6,6,14}][NTf_2]$.
Photographs and X-ray photoelectron spectra of the deposit surface (unmodified electrode; *green*) collected in the completely immersed area of the bare nickel wire electrode in the 2 M $LiNTf_2$ + 0.1 M $[P_{6,6,6,14}][NTf_2]$ tetrahydrofuran electrolyte solution. These data were collected for the electrode used in the Li-NRR experiment at -0.55 V *vs.* $Li^{0/+}_{app}$ in a single-compartment as those presented in the Figure S8c and 8g. Depth profiling for the deposit surface was achieved with different ion etching times from 0 to 1200 s (*tints of green*, see figure). XP spectra recorded for a freshly polished nickel wire electrode that was kept in 2 M $LiNTf_2$ + 0.1 M $[P_{6,6,6,14}][NTf_2]$ tetrahydrofuran solution for 6 h under 15 bar N_2 are shown for comparison as *black* traces. F KLL Auger signals manifest in the same binding energy range as Ni 2p. *Red* region indicates $[P_{6,6,6,14}]^+$ signal.

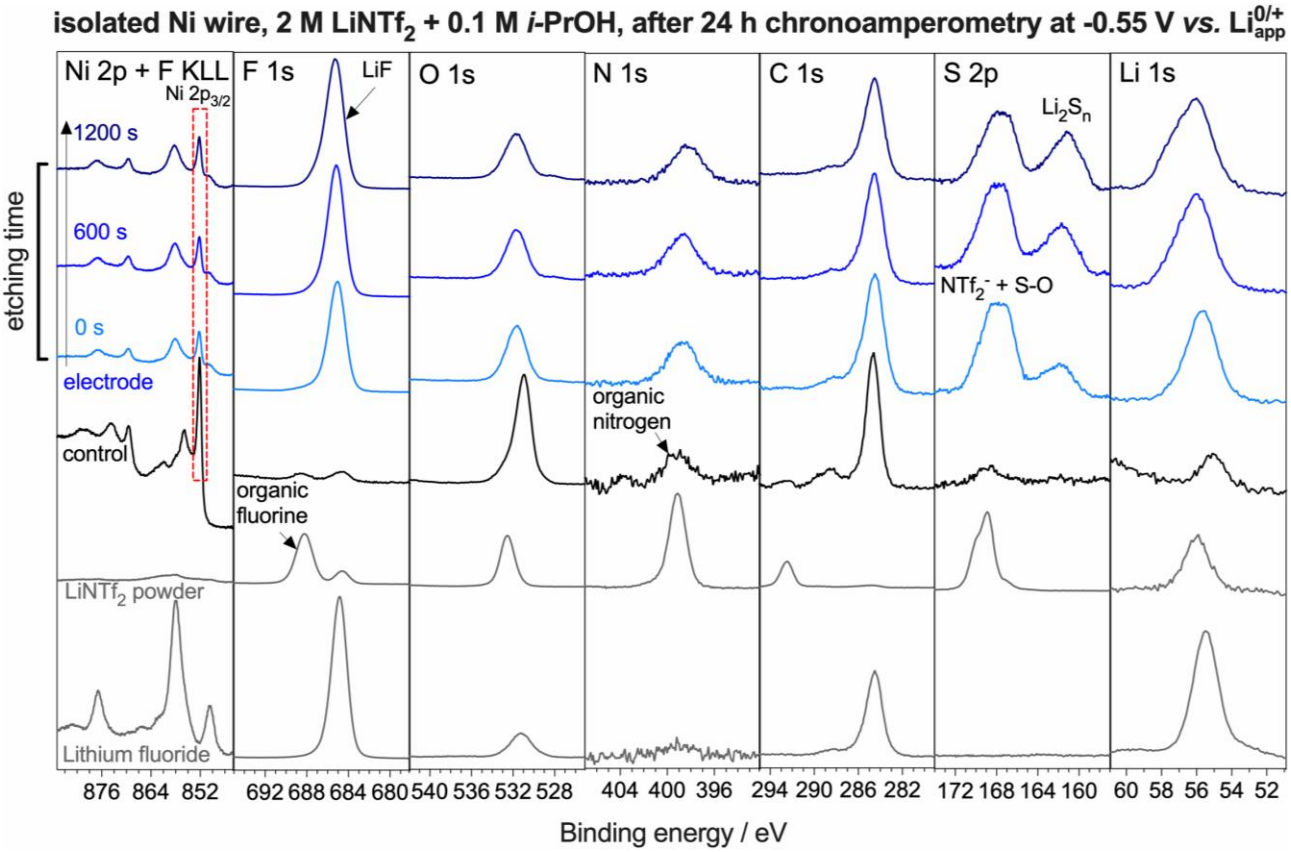

Figure S25. XPS analysis of the isolated Ni electrode after the Li-NRR with 0.1 M *i*-PrOH.
X-ray photoelectron spectra of the surface collected in the immersed part of the isolated nickel wire electrode in the 2 M $LiNTf_2$ + 0.1 M *i*-PrOH tetrahydrofuran electrolyte solution. These data were collected for the electrode used in the Li-NRR experiment at -0.55 V *vs.* $Li^{0/+}_{app}$ in a single-compartment as those presented in the Figure S28. Depth profiling of the electrode surface was achieved with different ion etching times from 0 to 1200 s (*tints of blue*, see figure). XP spectra recorded for a freshly polished nickel wire electrode that was kept in 2 M $LiNTf_2$ + 0.1 M *i*-PrOH tetrahydrofuran solution for 24 h under 15 bar N_2 are shown for comparison as *black* traces; data for $LiNTf_2$ powder and LiF powder are shown as *grey* curves. The signals of Ni $2p_{3/2}$ (*red* dashed box) separated from F KLL Auger signals were clearly detected on the electrode surface after the Li-NRR.

Electrolyte solutions

The ^{1}H NMR spectrum of the fresh 2 M $LiNTf_2$ + 0.1 M EtOH electrolyte solution features two main peaks of the tetrahydrofuran solvent at 2.09 and 3.94 ppm and peaks associated with ethanol (1.3 ppm (t, 3H), 3.7 ppm (m, 2h) and 4.8 ppm (t, 1H)) (Figure 3a). Spectra recorded after 3, 6, 9 and 12 h of the Li-NRR in a single-compartment system at -0.55 V *vs.* $Li^{0/+}_{app}$ under 15 bar N_2 feature new signals at 1.2 (t), 3.5 (m) and 5.2 ppm; additionally, the [OH] peak of ethanol was shifted and broadened (Figure 3a).

Complementary ^{13}C NMR spectra of the fresh electrolyte solution feature two main peaks of tetrahydrofuran at 25.5 and 68.0 ppm, two peaks of EtOH at 17.3 and 58.2 ppm, as well as [CF_3] signals of the NTf_2^- anion at 115.1, 118.3, 121.5 and 124.7 ppm (q). Upon completion of the chronoamperometric N_2 reduction experiments, new peaks at 14.6, 23.2, 32.1, 62.4, 66.6 and 103.7 ppm emerged (Figure S26a). ^{13}C NMR analysis of the electrolysed solutions in the DEPT-135 mode[18] indicates that the new peak at 103.7 ppm is associated with a tertiary-type carbon bonded to a single proton atom only (Figure S26a). In turn, signals at 52.1 and 42.9 ppm can be attributed to tetrahydrofuran, 58.1 and 17.2 ppm can be attributed to ethanol, while those at 14.6, 32.1 and 62.3 ppm are likely associated with the side product.

Next, a series of experiments was undertaken using deuterated compounds. After 12 h Li-NRR experiment with 0.1 M C_2D_5OD (deuterated EtOH) in tetrahydrofuran-h8, ^{1}H NMR spectra developed a new peak at 5.2 ppm in addition to the originally present solvent signals at 2.09 and 3.94 ppm (Figure S27a). Emergence of the peak at 5.2 ppm is attributed to the H/D exchange of the hydroxylic group of deuterated ethanol with the formation of C_2D_5OH. Broadening of the tetrahydrofuran peaks was also observed, which again suggests partial transformation of the solvent during the N_2 electroreduction experiment. Changes in the ^{2}H NMR spectra induced by the Li-NRR included disappearance of the [OD] signal due to the H/D exchange discussed above and emergence of new peaks at 1.2 and 3.5 ppm next to the [CD_2] and [CD_3] signals of deuterated EtOH (Figure S27b). New peaks developed in the ^{13}C NMR spectra after the Li-NRR test included signals at 23.2, 32.1, 66.6 and 103.7 ppm only (Figure S27c).

A set of tests was also carried out using tetrahydrofuran-d8 solvent and 0.1 M EtOH. In this case, ^{1}H NMR spectra of the fresh electrolyte solution features well-resolved ethanol peaks along with the signals of the unavoidable tetrahydrofuran-h8 admixture (Figure 3b). After a 12 h N_2 electroreduction test, two additional peaks at 1.3 ppm (t) and 3.6 ppm (m) were detected, similar to the experiments with a regular tetrahydrofuran solvent (Figure 3a). Additionally, new multiplet signal emerged at slightly lower chemical shifts than the [CH_2] ethanol peaks at 3.7 ppm. ^{2}H NMR spectra before and after the Li-NRR featured only two peaks of the deuterated solvent, which were broadened to some extent upon completion of the chronoamperometric test (Figure S28a). The latter observation suggests that tetrahydrofuran underwent partial chemical transformation(s) during the N_2 reduction experiment. ^{13}C NMR spectra of the tetrahydrofuran-d8 electrolyte solution recorded after the Li-NRR test featured only two new major peaks at 14.8 and 62.3 ppm (Figure S28b), but no clearly identifiable signals at 23.2, 32.1, 66.6 and 103.7 ppm which were detected for the electrolysed tetrahydrofuran-h8 solutions (Figure S26a and 27c).

Based on the outcomes of the experiments with the deuterated ethanol and tetrahydrofuran, we conclude that the side product(s) developing in the solution after the Li-NRR are associated with the transformations of ethanol (1.2-1.3 ppm (t) and 3.5-3.6 ppm (m) in ^{1}H NMR; 17.3 and 58.2 ppm in ^{13}C NMR) and tetrahydrofuran (23.2, 32.1, 66.6 and 103.7 ppm in ^{13}C NMR).

It is also important to note that no detectable degradation of the $[NTf_2]^-$ anion occurred during the Li-NRR (Figures S26b), confirming[3] that this anion is stable both cathodically and anodically during high-performance ammonia electrosynthesis.

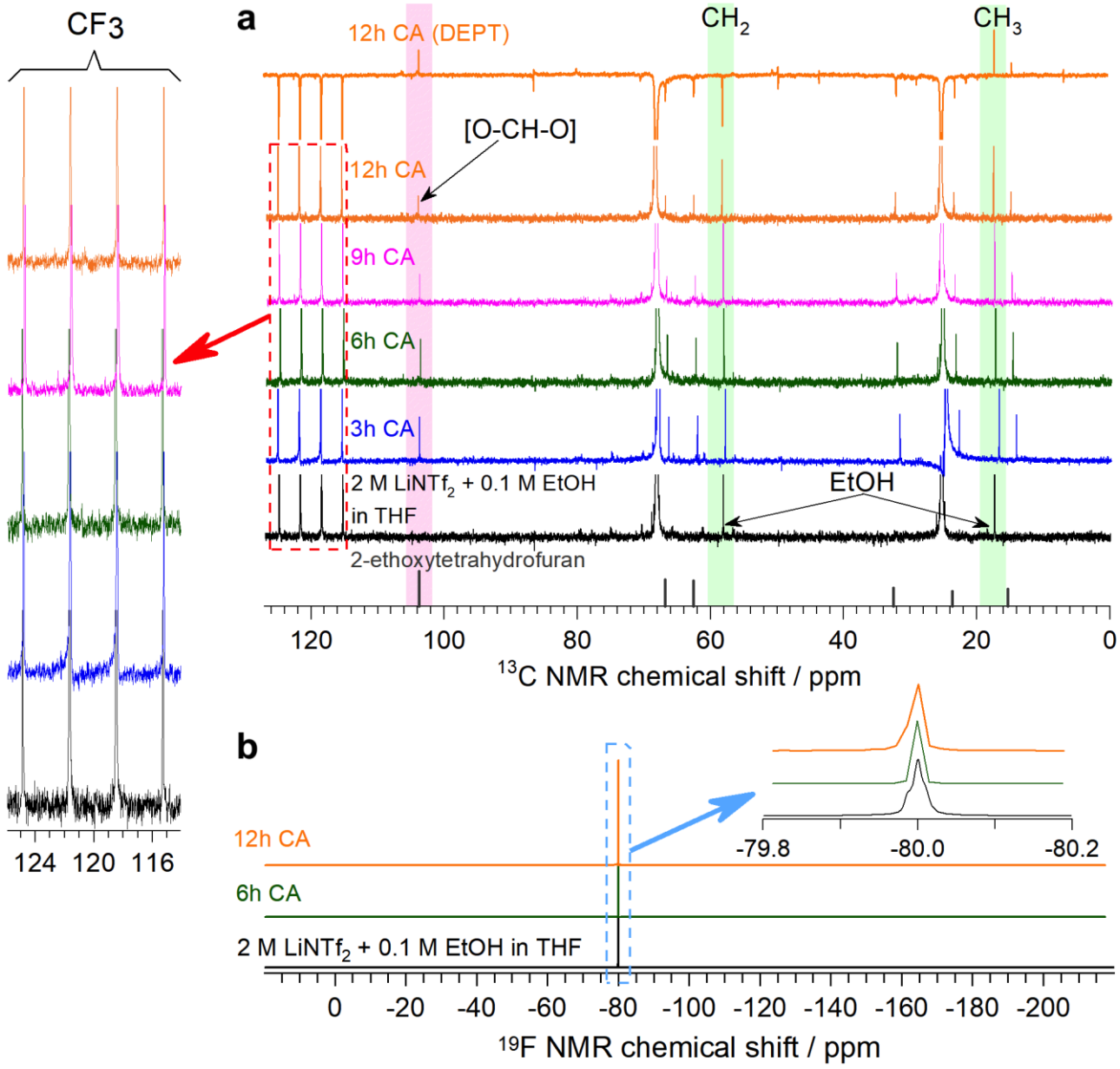

Figure S26. NMR analysis of fresh and tested 2 M $LiNTf_2$ + 0.1 M EtOH electrolyte solutions. (a) ^{13}C and (b) ^{19}F NMR analysis the tetrahydrofuran-h8 solutions before (*black*) and after 3 (*blue*), 6 (*green*), 9 (*magenta*) and 12 h (*orange*) electroreduction using a bare Ni wire electrode (0.15 cm^2) at -0.55 V *vs.* $Li^{0/+}_{app}$ under continuous stirring and 15 bar N_2 pressure in a single-compartment configuration. Insets show enhanced plots of peaks contained in *red* and *light blue* dashed boxes for ^{13}C and ^{19}F, respectively. In panel a, *green* and *pink* shadings highlight NMR signals from EtOH and [O-CH-O] functionality of 2-ethoxytetrahydrofuran, respectively, while *grey* vertical lines show data for 2-ethoxytetrahydrofuran from the AIST database.[19] No NMR signals were observed beyond the spectral regions shown.

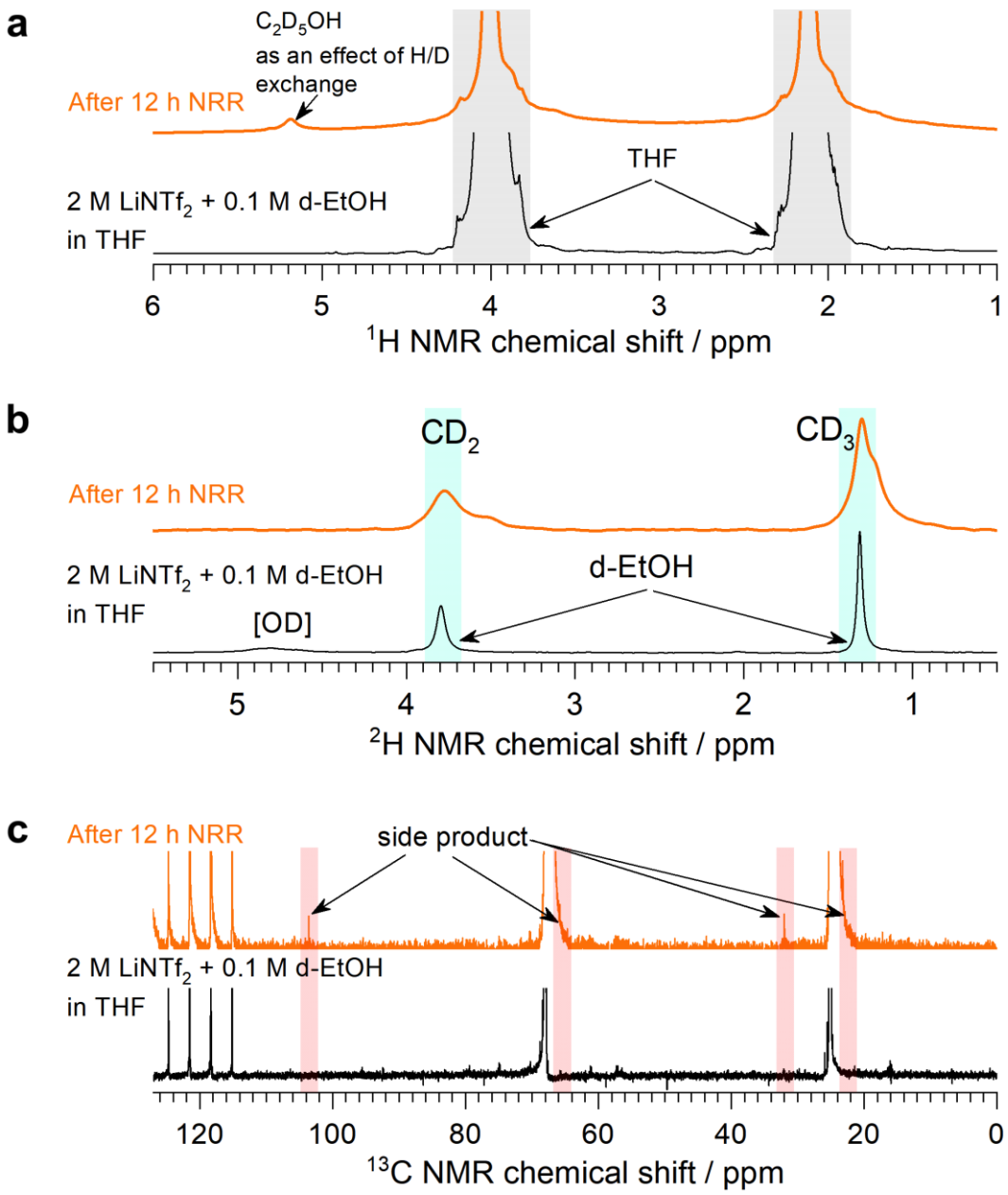

Figure S27. NMR analysis of fresh and tested 2 M $LiNTf_2$ + 0.1 M C_2D_5OD electrolyte solutions in tetrahydrofuran-h8.

(a) ^{1}H, (b) ^{2}D and (c) ^{13}C NMR spectra of the 2 M $LiNTf_2$ + 0.1 M C_2D_5OD electrolyte solutions in tetrahydrofuran-h8 before (*black*) and after (*orange*) 12 h electroreduction using a bare Ni wire electrode (0.15 cm^2) at -0.55 V *vs.* $Li^{0/+}_{app}$ under continuous stirring and 15 bar N_2 pressure in a single-compartment configuration.

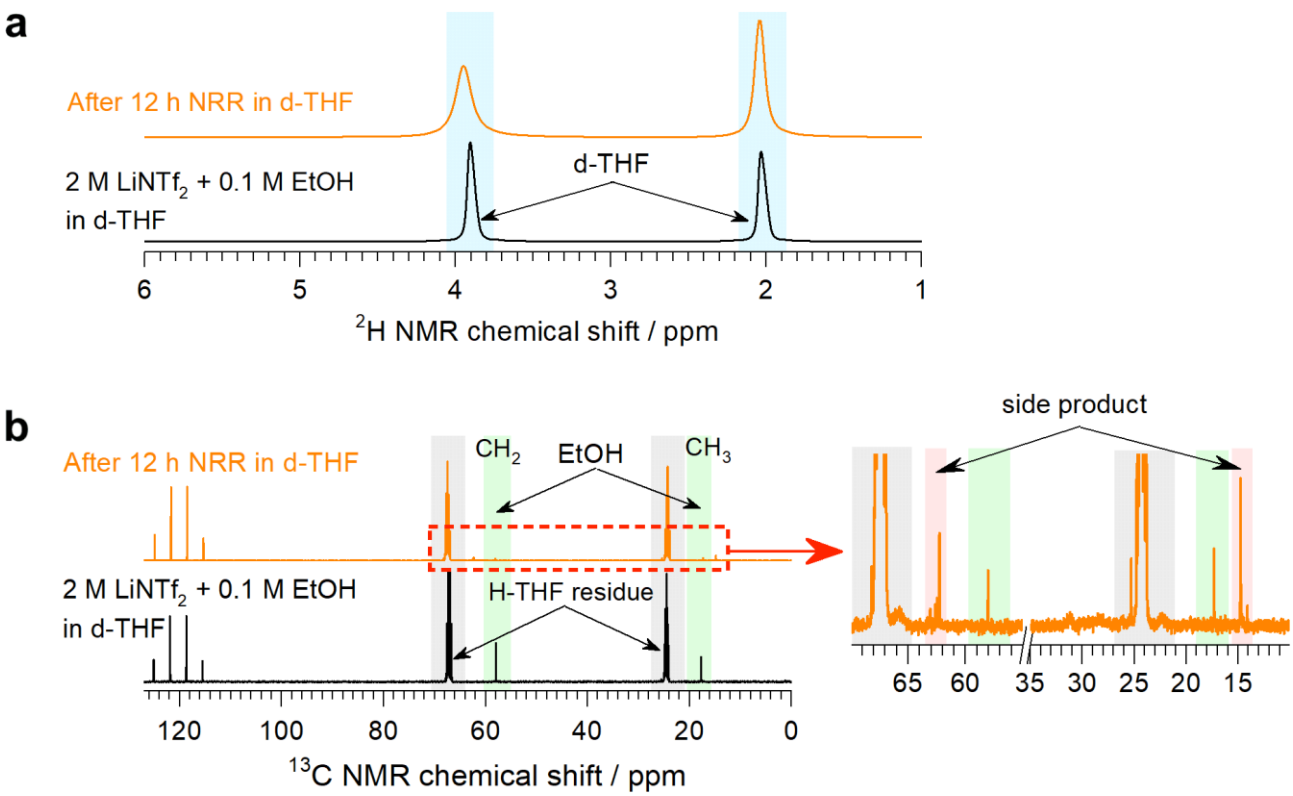

Figure S28. NMR analysis of fresh and tested 2 M $LiNTf_2$ electrolyte solutions with deuterated tetrahydrofuran.

(a) ^{2}H and (b) ^{13}C NMR analysis of the working 2 M $LiNTf_2$ + 0.1 M EtOH in tetrahydrofuran-d8 electrolyte solutions before (*black*) and after (*orange*) 12 h electroreduction using a bare Ni wire electrode (0.15 cm^2) at -0.55 V *vs.* $Li^{0/+}_{app}$ under continuous stirring and 15 bar N_2 pressure in a single-compartment configuration.

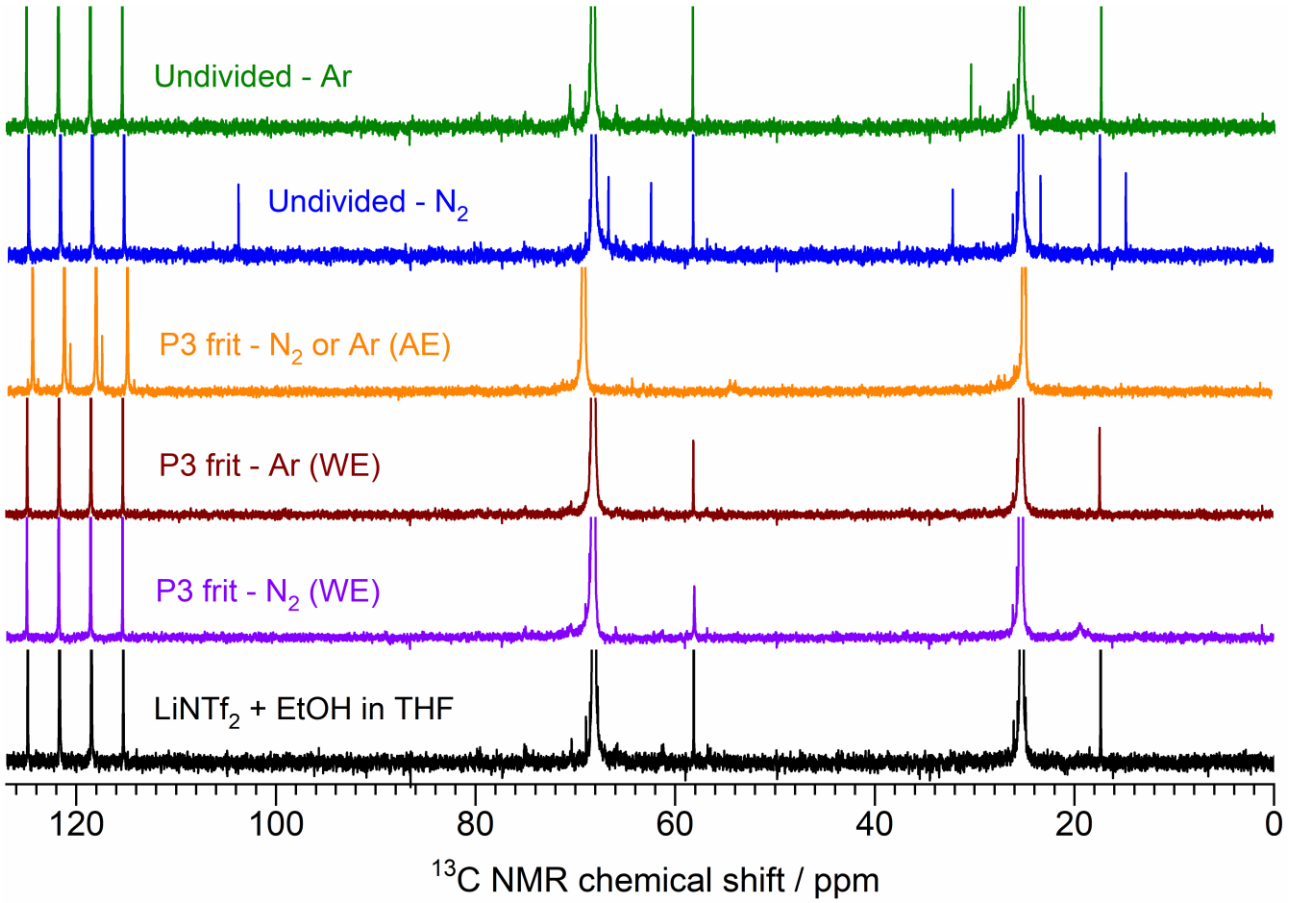

Figure S29. ^{13}C NMR of the electrolyte solutions derived from the Li-NRR with a single- and two-compartment cell configuration.

^{13}C NMR spectra of the 2 M Li[NTf_2] + 0.1 M EtOH tetrahydrofuran working electrolyte solutions before (*black*) and after 6 h chronoamperometric reduction at -0.55 V *vs.* $Li^{0/+}_{app}$ undertaken using a bare nickel wire electrode (0.15 cm^2) at 15 bar and the following conditions: under Ar in a single- (*green*) and two-compartment cell configuration (*wine*), under N_2 in a single- (*blue*) and two-compartment cell configuration (*purple*). Data for the 2 M $LiNTf_2$ tetrahydrofuran electrolyte solution from the auxiliary electrode compartment for the N_2 or Ar experiments are shown as *orange* trace.

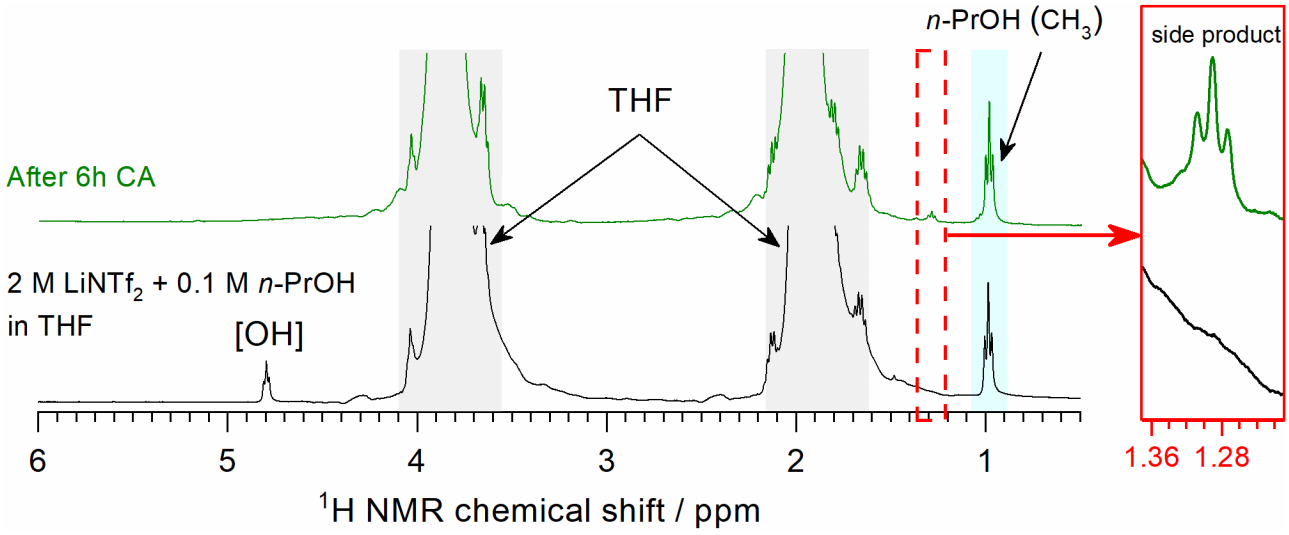

Figure S30. ^{1}H NMR analysis of fresh and tested 2 M $LiNTf_2$ + 0.1 M *n*-PrOH electrolyte solutions.

^{1}H NMR spectra of the 2 M $LiNTf_2$ + 0.1 M *n*-PrOH tetrahydrofuran working electrolyte solutions before (*black*) and after 6 (*green*) chronoamperometric reduction at -0.55 V *vs.* $Li^{0/+}_{app}$ undertaken using a bare nickel wire electrode (0.15 cm^2) at 15 bar N_2 in a single-compartment cell configuration. Inserts show the enhanced chemical shift of side product.

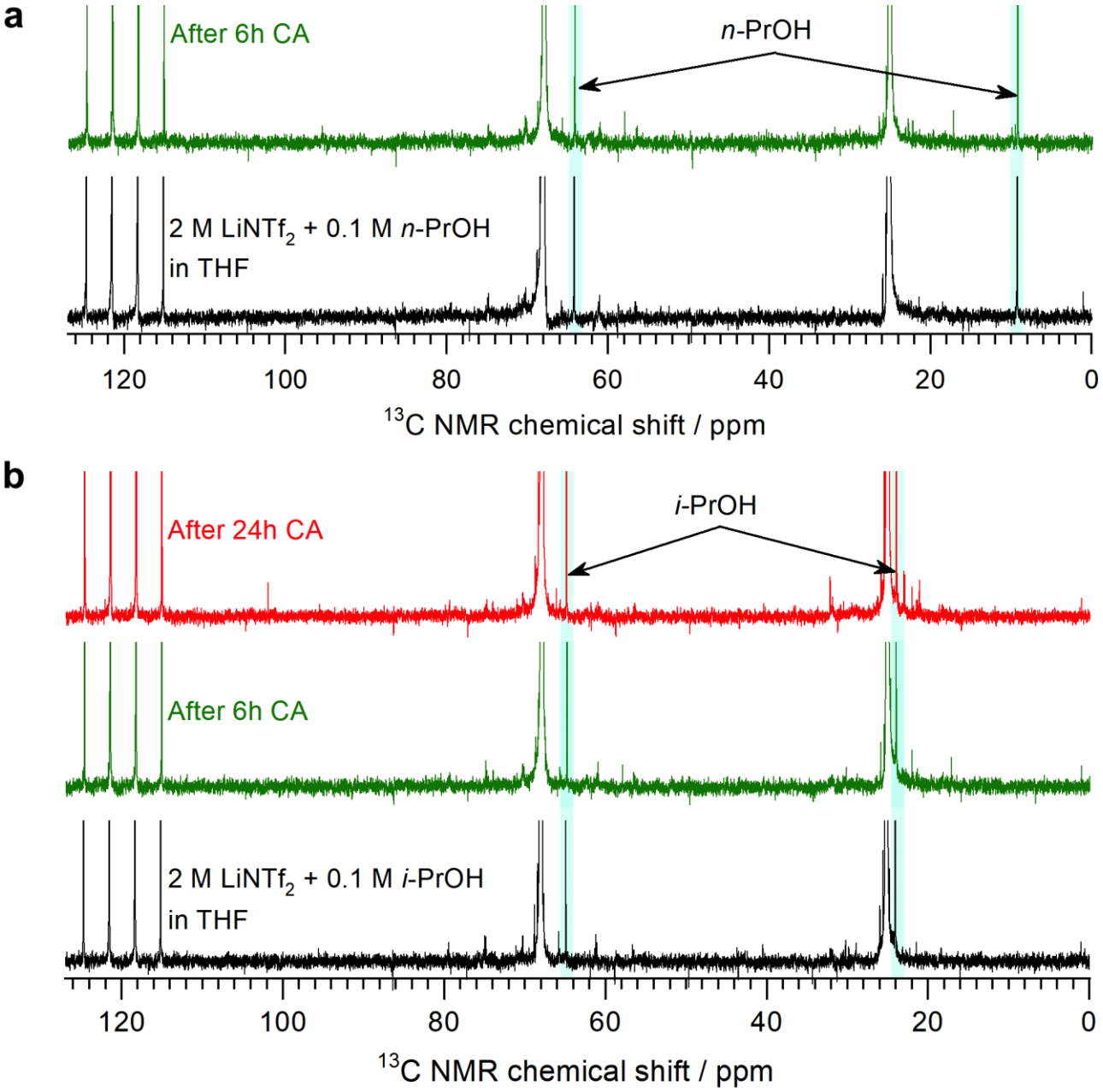

Figure S31. ^{13}C NMR analysis of fresh and tested 2 M $LiNTf_2$ + 0.1 M propanol electrolyte solutions.

^{13}C NMR spectra of the tetrahydrofuran working electrolyte solutions containing 0.1 M (a) *n*-PrOH and (b) *i*-PrOH before (*black*), after 6 (*green*) and 24 h (*red*) chronoamperometric reduction at -0.55 V *vs.* $Li^{0/+}_{app}$ undertaken using a bare nickel wire electrode (0.15 cm^2) (*green*) and an isolated nickel wire electrode (0.05 cm^2) (*red*) at 15 bar N_2 in a single-compartment cell configuration.

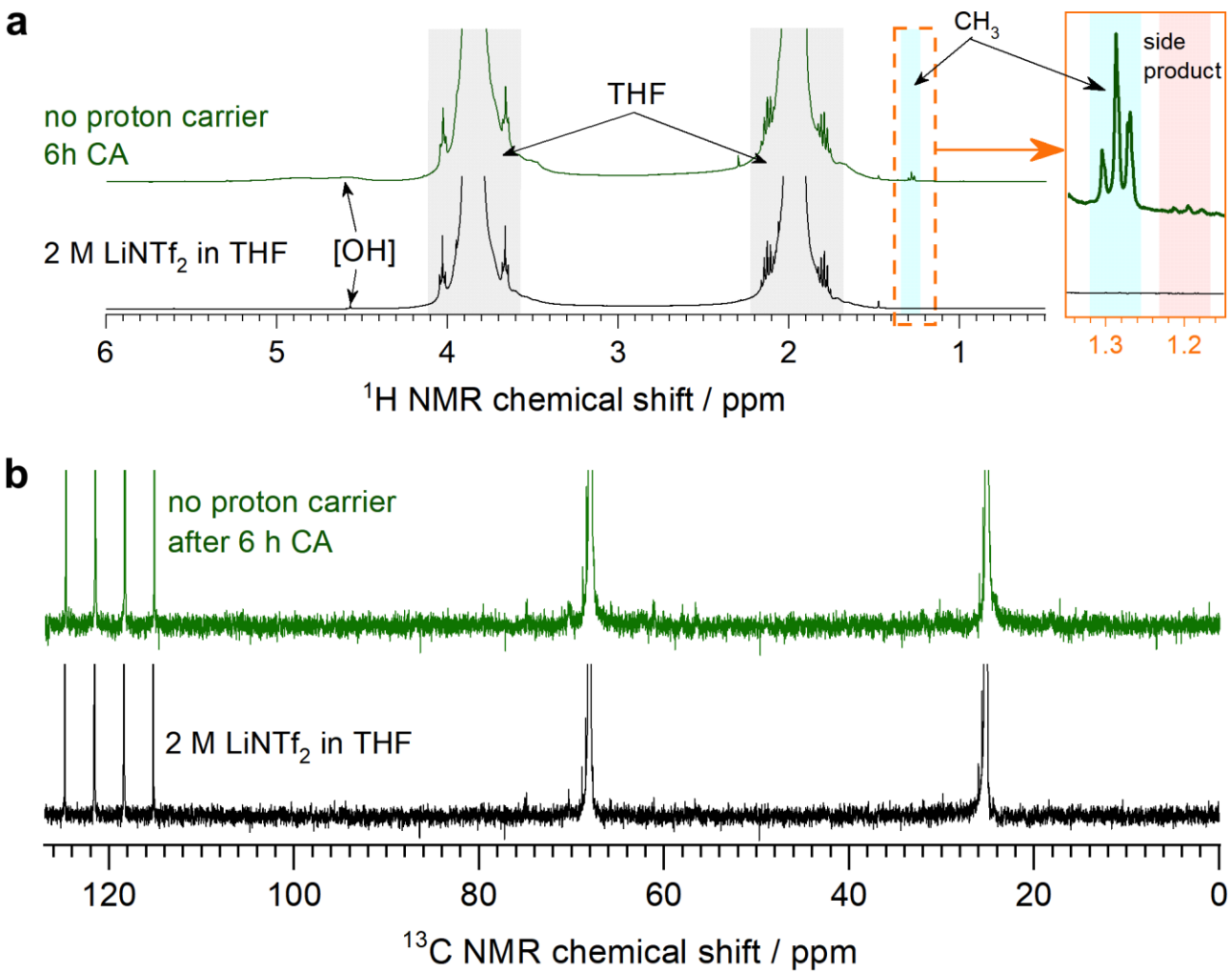

Figure S32. ^{1}H and ^{13}C NMR analysis of fresh and tested 2 M $LiNTf_2$ electrolyte solutions without added proton carriers.

(a) ^{1}H and (b) ^{13}C NMR spectra of the 2 M $LiNTf_2$ tetrahydrofuran working electrolyte solutions without added proton carriers before (*black*) and after 6 (*green*) and 24 h (*red*) chronoamperometric reduction at -0.55 V *vs.* $Li^{0/+}_{app}$ undertaken using a bare nickel wire electrode (0.15 cm^2) (*green*) and isolated nickel wire electrode (0.05 cm^2) (*red*) at 15 bar N_2 in a single-compartment cell configuration. Inserts show the enhanced chemical shift of side product.

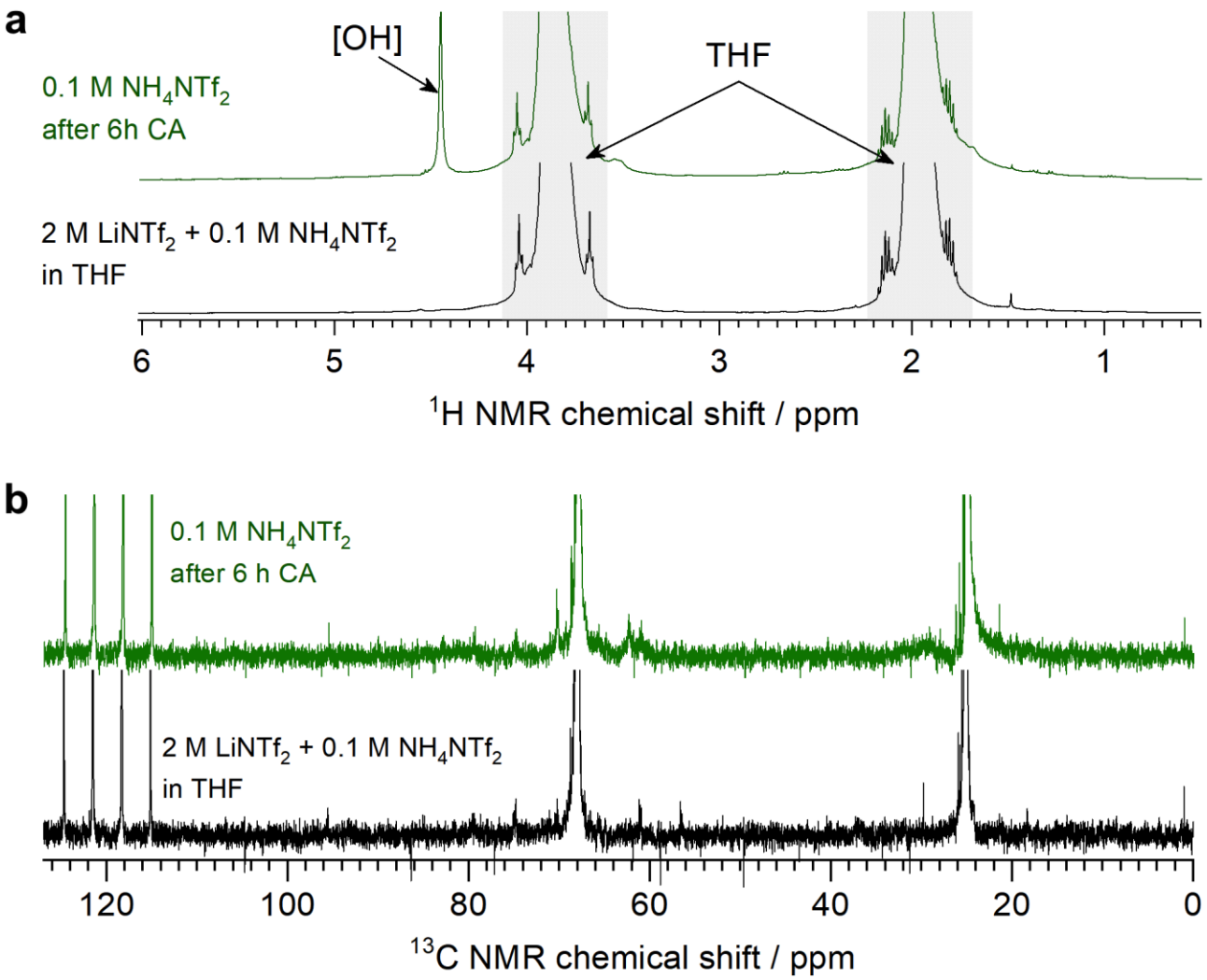

Figure S33. ^{1}H and ^{13}C NMR analysis of fresh and tested 2 M $LiNTf_2$ + 0.1 M NH_4NTf_2 electrolyte solutions.

(a) ^{1}H and (b) ^{13}C NMR spectra of the 2 M $LiNTf_2$ + 0.1 M NH_4NTf_2 tetrahydrofuran working electrolyte solutions without added proton carriers before (*black*) and after 6 (*green*) and 24 h (*red*) chronoamperometric reduction at -0.55 V *vs.* $Li^{0/+}_{app}$ undertaken using a bare nickel wire electrode (0.15 cm^2) (*green*) and isolated nickel wire electrode (0.05 cm^2) (*red*) at 15 bar N_2 in a single-compartment cell configuration.

5. EXTENDED DATA FOR 24 H EXPERIMENTS WITH ISOLATED NICKEL WIRE ELECTRODE

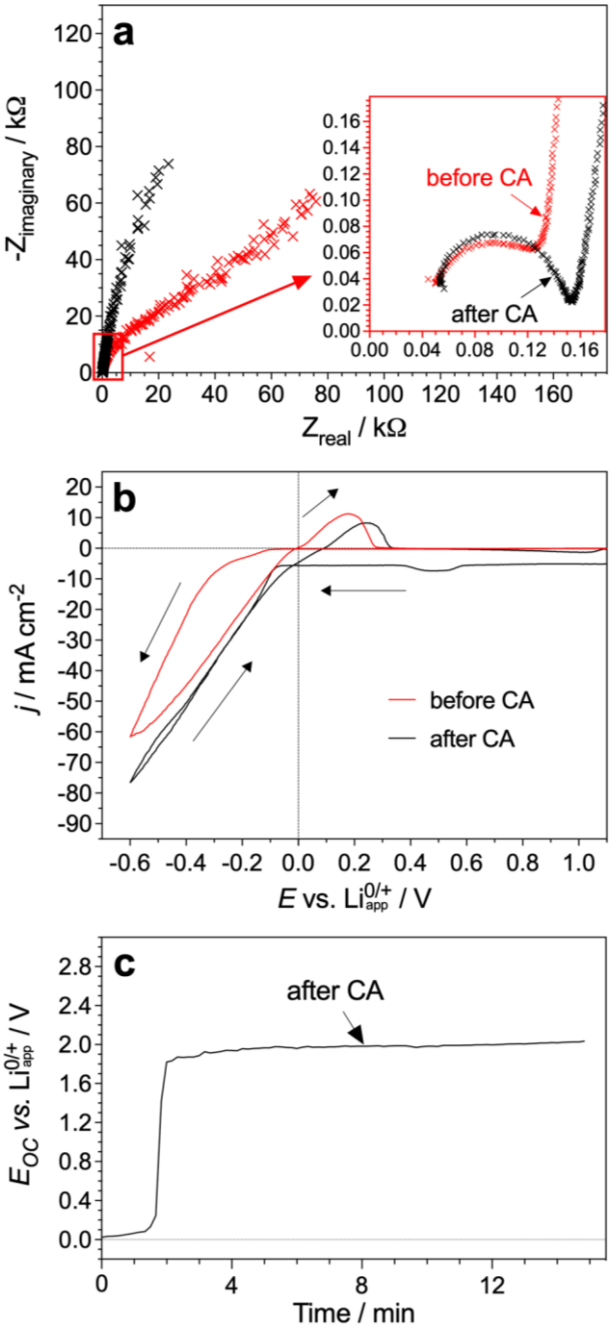

Figure S34. Extended electrochemical data for 24 h Li-NRR with 0.1 M *i*-PrOH.
(a) Electrochemical impedance spectroscopy measured at open circuit potential (insets show enhanced plots of the semi-circles for all concentrations), (b) cyclic voltammetry (0.020 V s^{-1}; 20th scan; arrows show the sweep direction), (c) and subsequent evolution of the working electrode open circuit potential before (*red*) and after (*black*) chronoamperometric tests at -0.55 V *vs.* $Li^{0/+}_{app}$ recorded for an isolated nickel wire electrode (0.05 cm^2) in 2 M $LiNTf_2$ along with 0.1 M *i*-PrOH. Horizontal dashed lines show j = 0 mA cm^{-2} while the vertical dashed line shows E = 0 V *vs.* $Li^{0/+}_{app}$. Solutions were not stirred during EIS, and continuously stirred during voltammetry and open circuit potential. Other conditions as in Figure S5.

6. SUPPLEMENTARY TABLES

Table S1. Summary of the data for the 6 h Li-NRR experiments with different proton carriers.[a]

H^+ carrier	α [b]	β [b]	C_{H+} / M	Charge / C	Total NH_3 / μmol [d]	Yield rate / nmol s^{-1} cm^{-2} [d]	Faradaic efficiency / % [d]
Tetrahydrofuran[c]	0	0.55	8.9	291	270 (C.I ± 20)	80 (C.I ± 6)	30 (C.I ± 2)
MeOH	0.98	0.66	0.1	164	80 (C.I ± 20)	30 (C.I ± 7)	14 (C.I ± 4)
EtOH	0.86	0.75	0.03	777	440 (C.I ± 50)	140 (C.I ± 14)	60 (C.I ± 6)
			0.1 [e]	252 ± 30 [e]	740 ± 70 [e]	230 ± 20 [e]	85 ± 8 [e]
			0.18	216	510 (C.I. ± 56)	160 (C.I. ± 17)	68 (C.I. ± 7)
				231	680 (C.I. ± 50)	130 (C.I. ± 9)	85 (C.I. ± 6)
				194	600 (C.I. ± 60)	110 (C.I. ± 11)	90 (C.I. ± 9)
			0.72	19	3 (C.I. ± 3)	0.8 (C.I. ± 1)	4 (C.I. ± 5)
n-PrOH	0.84	0.9	0.03	300	610 (C.I. ± 50)	190 (C.I. ± 20)	59 (C.I. ± 5)
			0.07	310	700 (C.I. ± 10)	220 (C.I. ± 4)	65 (C.I. ± 1)
			0.1	292	770 (C.I. ± 20)	240 (C.I. ± 6)	76 (C.I. ± 2)
			0.2	120	270 (C.I. ± 30)	80 (C.I. ± 9)	70 (C.I. ± 7)
			0.4	70	100 (C.I. ± 7)	30 (C.I. ± 2)	40 (C.I. ± 3)

[a] Experiments were undertaken for 6 h using a bare Ni wire electrode at -0.55 V *vs.* $Li^{0/+}_{app}$ in stirred 2 M $Li[NTf_2]$ tetrahydrofuran solutions containing defined concentration of the proton carrier and saturated with N_2 at 15 bar. [b] Kamlet-Taft parameters from references.[20, 21] [c] No proton carrier was added. [d] C.I. ± values indicate the 95% confidence intervals for the ammonia measurement by the method of standard additions. [e] Data are shown as mean ± one standard deviation obtained from n = 10 repeats of the experiments reported previously.[3]

Table S1. Summary of the data for the 6 h Li-NRR experiments with different proton carriers (continued).[a]

H^+ carrier	α [b]	β [b]	C_{H+} / M	Charge / C	Total NH_3 / μmol [d]	Yield rate / nmol s^{-1} cm^{-2} [d]	Faradaic efficiency / % [d]
i-PrOH	0.76	0.84	0.03	262	570 (C.I. ± 30)	176 (C.I. ± 9)	63 (C.I. ± 3)
			0.07	295	740 (C.I. ± 20)	230 (C.I. ± 7)	73 (C.I. ± 2)
			0.1	274	700 (C.I. ± 60)	220 (C.I. ± 20)	74 (C.I. ± 7)
			0.2	196	450 (C.I. ± 20)	140 (C.I. ± 6)	67 (C.I. ± 3)
			0.4	72	106 (C.I. ± 10)	33 (C.I. ± 3)	43 (C.I. ± 4)
n-BuOH	0.84	0.84	0.1	150	340 (C.I. ± 60)	104 (C.I. ± 20)	65 (C.I. ± 10)
n-PeOH	0.84	0.86	0.1	195	280 (C.I. ± 20)	90 (C.I. ± 5)	42 (C.I. ± 3)
$[P_{6,6,6,14}][eFAP]$	0.20	1.24	0.03	331	340 (C.I. ± 10)	106 (C.I. ± 3)	30 (C.I. ± 1)
			0.07	368	430 (C.I. ± 6)	130 (C.I. ± 2)	34 (C.I. ± 1)
			0.1	201	280 (C.I. ± 8)	90 (C.I. ± 3)	40 (C.I. ± 1)
				260	440 (C.I. ± 30)	140 (C.I. ± 9)	50 (C.I. ± 3)
				228	470 (C.I. ± 50)	150 (C.I. ± 15)	60 (C.I. ± 6)
			0.2	190	290 (C.I. ± 14)	90 (C.I. ± 4)	44 (C.I. ± 2)
			0.3	120	150 (C.I. ± 8)	45 (C.I. ± 3)	35 (C.I. ± 2)
			0.55	6	0.3 (C.I. ± 0.05)	0.1 (C.I. ± 0.02)	2 (C.I. ± 0.3)
$[P_{6,6,6,14}][NTf_2]$	0.20	1.24	0.03	355	200 (C.I. ± 30)	70 (C.I. ± 10)	16 (C.I. ± 3)
			0.1	315	440 (C.I. ± 50)	140 (C.I. ± 14)	40 (C.I. ± 4)
			0.3	167	180 (C.I. ± 20)	56 (C.I. ± 6)	31 (C.I. ± 3)
			0.4	110	93 (C.I. ± 12)	33 (C.I. ± 4)	24 (C.I. ± 3)

[a] Experiments were undertaken for 6 h using a bare Ni wire electrode at -0.55 V *vs.* $Li^{0/+}_{app}$ in stirred 2 M $LiNTf_2$ tetrahydrofuran solutions containing defined concentration of the proton carrier and saturated with N_2 at 15 bar. [b] Kamlet-Taft parameters from references.[20, 21] [c] No proton carrier was added. [d] C.I. ± values indicate the 95% confidence intervals for the ammonia measurement by the method of standard additions. [e] Data are shown as mean ± one standard deviation obtained from n = 10 repeats of the experiments reported previously.[3]

Table S1. Summary of the data for the 6 h Li-NRR experiments with different proton carriers (continued).[a]

H^+ carrier	α [b]	β [b]	C_{H+} / M	Charge / C	Total NH_3 / μmol [d]	Yield rate / nmol s^{-1} cm^{-2} [d]	Faradaic efficiency / % [d]
$HNTf_2$	>> 1	Not available	0.001	240	70 (C.I. ± 40)	20 (C.I. ± 12)	9 (C.I. ± 5)
			0.01	430	300 (C.I. ± 40)	90 (C.I. ± 12) [e]	20 (C.I. ± 3) [e]
				220	140 (C.I. ± 13)	40 (C.I. ± 4)	18 (C.I. ± 2)
				330	210 (C.I. ± 13)	70 (C.I. ± 4)	19 (C.I. ± 1)
			0.015	160	170 (C.I. ± 6)	50 (C.I. ± 2)	30 (C.I. ± 1)
			0.02	120	160 (C.I. ± 40)	48 (C.I. ± 12)	40 (C.I. ± 9)
			0.04	120	100 (C.I. ± 7)	30 (C.I. ± 2)	24 (C.I. ± 2)
			0.1	390	14 (C.I. ± 10)	4 (C.I. ± 3)	1 (C.I. ± 0.7)
H_2O	1.17	0.47	0.1	830	14 (C.I. ± 8)	4 (C.I. ± 2)	0.5 (C.I. ± 0.3)
NH_4NTf_2	Not available	Not available	0.1	840	240 (C.I. ± 70)	20 (C.I. ± 5)	8 (C.I. ± 2)
				938	310 (C.I. ± 40)	24 (C.I. ± 3)	10 (C.I. ± 1)

[a] Experiments were undertaken for 6 h using a bare Ni wire electrode at -0.55 V *vs.* $Li^{0/+}_{app}$ in stirred 2 M $LiNTf_2$ tetrahydrofuran solutions containing defined concentration of the proton carrier and saturated with N_2 at 15 bar. [b] Kamlet-Taft parameters from references.[20, 21] [c] No proton carrier was added. [d] C.I. ± values indicate the 95% confidence intervals for the ammonia measurement by the method of standard additions. [e] Data are shown as mean ± one standard deviation obtained from n = 10 repeats of the experiments reported previously.[3]

Table S2. Summary of the data for the 6 h Li-NRR experiments with 0.1 M $[P_{6,6,6,14}]$[eFAP] and different concentrations of $LiNTf_2$.[a]

$C_{[LiNTf_2]}$ / M	Charge / C	Total NH_3 / µmol [b]	Yield rate / nmol s^{-1} cm^{-2} [b]	Faradaic efficiency / % [b]
0.5	134	20 (C.I. ± 2)	6 (C.I. ± 0.5)	4 (C.I. ± 0.3)
0.75	250	270 (C.I. ± 20)	80 (C.I. ± 5)	30 (C.I. ± 2)
1	190	460 (C.I. ± 40)	140 (C.I. ± 10)	77 (C.I. ± 6)
	167	450 (C.I. ± 11)	150 (C.I. ± 4)	78 (C.I. ± 2)
	164	440 (C.I. ± 10)	140 (C.I. ± 4)	78 (C.I. ± 2)
1.5	242	550 (C.I. ± 30)	170 (C.I. ± 9)	66 (C.I. ± 3)
2	201	280 (C.I. ± 8)	90 (C.I. ± 3)	40 (C.I. ± 1)
	259	440 (C.I. ± 30)	140 (C.I. ± 9)	50 (C.I. ± 3)
	228	470 (C.I. ± 50)	145 (C.I. ± 15)	60 (C.I. ± 6)

[a] Experiments were undertaken for 6 h using a bare Ni wire electrode (0.15 cm^2) at -0.55 V *vs.* $Li^{0/+}_{app}$ in stirred $LiNTf_2$ + 0.1 M $[P_{6,6,6,14}]$[eFAP] tetrahydrofuran electrolyte solutions saturated with N_2 at 15 bar. [b] C.I. ± values indicate the 95% confidence intervals for the ammonia measurement by the method of standard additions.

Table S3. Summary of the data for the Li-NRR experiments with different cell configurations.[a]

Configuration	*t* / h	Charge / C	Total NH_3 / μmol [b]	Yield rate / nmol s^{-1} cm^{-2} [b]	Faradaic efficiency / % [b]
Single compartment	3 [c]	146 ± 3 [c]	340 ± 40 [c]	210 ± 30 [c]	67 ± 7 [c]
	6 [c]	252 ± 30 [c]	740 ± 70 [c]	230 ± 20 [c]	85 ± 8 [c]
Two compartments	3	133	290 (C.I. ± 28)	180 (C.I. ± 17)	63 (C.I. ± 6)
		102	270 (C.I. ± 19)	170 (C.I. ± 11)	77 (C.I. ± 5)
		104	330 (C.I. ± 41)	200 (C.I. ± 25)	91 (C.I. ± 11)
	6	161	520 (C.I. ± 20)	160 (C.I. ± 6)	94 (C.I. ± 4)
		155	330 (C.I. ± 24)	100 (C.I. ± 7)	62 (C.I. ± 5)
		165	460 (C.I. ± 45)	140 (C.I. ± 14)	81 (C.I. ± 8)
		167	540 (C.I. ± 62)	170 (C.I. ± 19)	94 (C.I. ± 11)

[a] Experiments were undertaken for a defined period of time using a bare Ni wire electrode at -0.55 V *vs.* $Li^{0/+}_{app}$ in stirred 2 M $LiNTf_2$ + 0.1 M EtOH tetrahydrofuran electrolyte solutions saturated with N_2 at 15 bar in single- or two-compartment cell configuration. [b] C.I. ± values indicate the 95% confidence intervals for the ammonia measurement by the method of standard additions. [c] ± values indicate mean and one standard deviation obtained from our previous study.[3]

Table S4. Summary of the data for 24 h Li-NRR experiments with isolated Ni wire electrodes.[a]

H^+ carrier	C_{H+} / M	Charge / C	Total NH_3 / μmol [b]	Yield rate / nmol s^{-1} cm^{-2} [b]	Faradaic efficiency / % [b]
EtOH	0.1	670 ± 20 [c]	2290 ± 70 [c]	530 ± 20 [c]	98 ± 2 [c]
i-PrOH	0.1	552	1830 (C.I. ± 70)	420 (C.I. ± 20)	96 (C.I. ± 4)
		600	2000 (C.I. ± 90)	460 (C.I. ± 20)	97 (C.I. ± 4)
		522	1700 (C.I. ± 30)	400 (C.I. ± 10)	95 (C.I. ± 2)
Mean (*n* = 3)				430	96
Standard deviation (*n* = 3)				± 20	± 1

[a] Experiments were undertaken for 24 h using an isolated Ni wire electrode (0.05 cm^2) at -0.55 V *vs.* $Li^{0/+}_{app}$ in stirred 2 M $LiNTf_2$ tetrahydrofuran electrolyte solutions saturated with N_2 at 15 bar. [b] C.I. ± values indicate the 95% confidence intervals for the ammonia measurement by the method of standard additions. [c] Data are shown as mean ± one standard deviation obtained from *n* = 4 repeats of the experiments reported previously.[3]

7. REFERENCES

1. B. H. Suryanto, K. Matuszek, J. Choi, R. Y. Hodgetts, H.-L. Du, J. M. Bakker, C. S. Kang, P. V. Cherepanov, A. N. Simonov and D. R. MacFarlane, *Science*, 2021, **372**, 1187-1191.
2. H. Pan, K. S. Han, M. H. Engelhard, R. Cao, J. Chen, J.-G. Zhang, K. T. Mueller, Y. Shao and J. Liu, *Adv. Funct. Mater.*, 2018, **28**, 1707234.
3. H.-L. Du, M. Chatti, R. Y. Hodgetts, P. V. Cherepanov, C. K. Nguyen, K. Matuszek, D. R. MacFarlane and A. N. Simonov, *Nature*, 2022, **609**, 722-727.
4. P. L. Searle, *Analyst*, 1984, **109**, 549-568.
5. R. Y. Hodgetts, A. S. Kiryutin, P. Nichols, H.-L. Du, J. M. Bakker, D. R. Macfarlane and A. N. Simonov, *ACS Energy Lett*, 2020, **5**, 736-741.
6. P. V. Cherepanov, M. Krebsz, R. Y. Hodgetts, A. N. Simonov and D. R. MacFarlane, *J. Phys. Chem. C*, 2021, **125**, 11402-11410.
7. E. P. Serjeant and B. Dempsey, *IUPAC chemical data series*, 1979, **23**, 160-190.
8. J. Riddick, W. Bunger and T. Sakano, *John Wiley and Sons: New York, NY*, 1985.
9. I. D. Weiner and J. W. Verlander, *Am. J. Physiol. Renal Physiol.*, 2011, **300**, F11-F23.
10. T. P. Silverstein and S. T. Heller, *J. Chem. Educ.*, 2017, **94**, 690-695.
11. W. Zhao and J. Sun, *Chem. Rev.*, 2018, **118**, 10349-10392.
12. O. A. O. Alshammari, G. A. A. Almulgabsagher, K. S. Ryder and A. P. Abbott, *Green Chem.*, 2021, **23**, 5097-5105.
13. N. Lazouski, M. Chung, K. Williams, M. L. Gala and K. Manthiram, *Nat. Catal.*, 2020, **3**, 463-469.
14. S. Z. Andersen, M. J. Statt, V. J. Bukas, S. G. Shapel, J. B. Pedersen, K. Krempl, M. Saccoccio, D. Chakraborty, J. Kibsgaard, P. C. K. Vesborg, J. Nørskov and I. Chorkendorff, *Energy Environ. Sci.*, 2020, **13**, 4291-4300.
15. K. Li, Z. Andersen Suzanne, J. Statt Michael, M. Saccoccio, J. Bukas Vanessa, K. Krempl, R. Sažinas, B. Pedersen Jakob, V. Shadravan, Y. Zhou, D. Chakraborty, J. Kibsgaard, C. K. Vesborg Peter, K. Nørskov Jens and I. Chorkendorff, *Science*, 2021, **374**, 1593-1597.
16. K. Li, S. G. Shapel, D. Hochfilzer, J. B. Pedersen, K. Krempl, S. Z. Andersen, R. Sažinas, M. Saccoccio, S. Li, D. Chakraborty, J. Kibsgaard, P. C. K. Vesborg, J. K. Nørskov and I. Chorkendorff, *ACS Energy Lett*, 2022, **7**, 36-41.
17. D. W. Jeppson, J. L. Ballif, W. W. Yuan and B. E. Chou, Lithium literature review: lithium's properties and interactions, United States, 1978.
18. Multinuclear NMR, Spinger US, 1 edn.
19. AIST: Integrated Spectral Database System of Organic Compounds., https://sdbs.db.aist.go.jp/sdbs/cgi-bin/direct_frame_top.cgi.
20. D. Krishnamurthy, N. Lazouski, M. L. Gala, K. Manthiram and V. Viswanathan, *ACS Cent. Sci.*, 2021, **7**, 2073-2082.
21. J. M. Padró and M. Reta, *J. Mol. Liq.*, 2016, **213**, 107-114.